공학석사 학위논문

Characterization of Rail Gun Plasmas for Simulating Edge Localized Mode Plasma

ELM 플라즈마 모사를 위한 레일건 플라즈마의 특성에 대한 연구

2013 년 2 월

서울대학교 대학원

에너지시스템공학부

정 경 수

Characterization of Rail Gun Plasmas for Simulating Edge Localized Mode Plasma

지도교수 황 용 석

이 논문을 공학석사 학위논문으로 제출함

2012 년 10 월

서울대학교 대학원

에너지시스템공학부

정 경 수

정경수의 공학석사 학위논문을 인준함

2012 년 12 월

위 원 장 김 곤 호 (인)

부 위 원 장 황 용 석 (인)

위 원 정 경 재 (인)

Abstract

Characterization of Rail Gun Plasmas for Simulating Edge Localized Mode Plasma

Kyoung Soo Chung

Department of Energy System Engineering

The Graduate School

Seoul National University

Damages of divertor targets by plasma loads during edge localized modes (ELMs) are critical issue in fusion engineering because they reduce the lifetime of the divertor target. In the case of ITER, the plasma load on divertor target during ELM is up to tens of GW/m^2 and its duration is approximately a few hundred microseconds. To evaluate the damages of divertor target during ELMs experimentally, various irradiation systems using a pulsed laser or particle beams have been proposed and tested. Among them, a pulsed plasma gun is thought to be suitable to simulate the ELM situation because it can give the particle load as well as the thermal heat load on the divertor target. Therefore, in this thesis, a small-sized rail gun is adopted to simulate the heat loads during ELMs and explore how to relieve the heat loads.

The rail gun is designed and fabricated in configuration of two parallel electrodes: the separation between the electrodes is 1 cm wide and the length of the rail is 30 cm long. The rail gun is installed at the top of cylindrical chamber so that the plasma jet is ejected vertically downward from the muzzle of the rail gun. The electrical current is fed to the electrodes by fast discharge of electrical energy stored in low-inductance capacitor. Initiation of discharge is accomplished by fast injection of gas at the breech of the rail using a piezoelectric valve. Argon and hydrogen are used as working gases.

Diagnostics of the plasma jet ejected from the muzzle of the rail gun is carried out with a quadruple Langmuir probe and a fast camera. The fast camera is also used to diagnose the formation and motion of the plasma channel between the electrodes, revealing almost linear increase in velocity with time. Dynamic motion of the plasma channel inside the rail is confirmed by a simple equivalent circuit model for parallel-plate rail gun, showing good agreements between the numerical calculation and the experimental observation. The quadruple Langmuir probe is used to measure the spatio-temporal changes for the properties of the plasma jet during the propagation in open space by moving the probe position vertically. With appropriate data processing, it provides the information on the time-dependent plasma properties, i.e. electron density, electron temperature and ion drift velocity, which are critical in studying the ELM-like plasmas.

From a lot of experiments conducted using gases with large difference in mass, i.e. hydrogen and argon, it is suggested that the plasma gun developed in this study can be separately applicable for the different topics on researches of ELM plasma: ELM control experiments for argon and heat load tests for hydrogen. The argon plasma jet with ion velocity of 10 km/s is suitable for investigation of the control of ELM-like plasma because the ion drift velocity is similar to the ELM filament velocity approaching to the divertor target. While, the ion drift velocity for the hydrogen plasma jet is much higher up to 120 km/s, so that it is possible to use for simulating the heat load impacting on the divertor surface. The ion drift velocity, or equivalently ion kinetic energy, is easily increased by increasing the length of the rail as well as the discharge current. Therefore,

the plasma gun developed and characterized in the present study is expected to be well utilized for the versatile researches on the future experiments on the ELM control and mitigation.

keywords : Rail gun, ELM plasma, Plasma jet, Quadruple Langmuir probe, PIC simulation, ELM control

student number : 2011-21107

Contents

List of Tables

List of Figures

Chapter 1 Introduction

1.1 Research motivation and objectives

The H-mode is essential as a regime of enhanced confinement in toroidal magnetic fusion devices [1, 2]. The edge localized mode, or ELM of the tokamak instabilities is a transient event which can lead to a repetitive loss of energy at the H-mode plasma edge. These transient heat loads, thousands of MW/m^2 are more critical when compared with the static heat loads during normal operation [3]. So far, the ELM has been serious problem in tokamak, because the H-mode operation having ELM is still regarded as the reference operational scenario for ITER. For this reason, understanding the ELM phenomena is important in tokamaks, and it provides a strong motivation for study of ELM.

Damages of divertor targets by plasma loads during the ELM are also critical issue in fusion engineering, because they reduce the lifetime of the divertor target. In the case of ITER, the plasma load on divertor target during type I ELM is up to tens of GW/m^2 and its duration is approximately a few hundred microseconds. Because of the high heat loads on divertor, it has been concerned with investigation of an erosion of the ITER-like divertor plasma facing materials under plasma heat loads expected during the type I ELM in ITER [4]. Eventually, the researches about the plasma facing component have been progressed by the heat load test utilizing the beam accelerators or thermal plasma torch such as QSPA [5], MCPG [6], ESP-gun [7], and Magnum-PSI [8].

Devices above-mentioned, however, are limitedly used as an ELM plasma simulator for testing the plasma facing component with their high heat flux and power. In other words, the machines cannot be called to ELM plasma simulator strictly, since they did not make ELM-like plasmas, but the high heat flux. Their goal was to select a proper plasma facing material though the heat flux test on the targets.

Figure 1.1 shows the conceptual diagram of a newly proposed control method for high heat load of ELM plasma. It is noted that the ELM-like plasma jet can be made in specific conditions via a pulsed plasma gun, and the jet can be used to explore how to control the plasma bunches before hitting the plasma facing materials so as to relieve the heat load. This concept of the control is different from pellet pacing [9], and resonant magnetic perturbation [10] in terms of the particles control of type I ELM plasma with external fields.

The construction of a plasma gun is essential to realize the concept in order to product a plasma jet. The concept of the rail gun in vacuum is adopted to represent the plasma gun. The gun includes both electron and ion similar to ELM, and it has simple structure and low cost. Therefore, it is considered to be suitable to simulate the plasma parameters such as temperature, density, velocity during ELM.

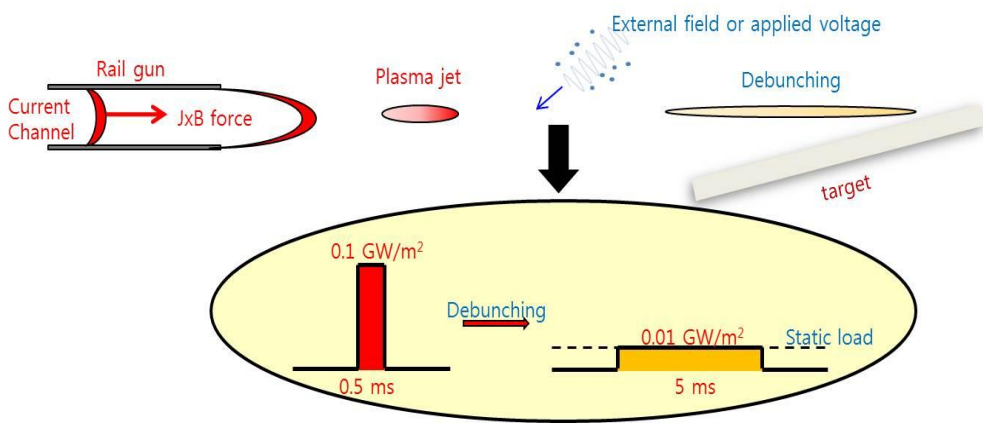

Figure 1.1 Conceptual diagram of a newly proposed control method for high heat load of ELM plasma.

The measurements on the properties of the plasma jets are essential because the changes of plasma properties by external active or passive controls are a measure of the effectiveness of control. In order to measure plasma properties of plasma jet in rail gun, two kinds of diagnostic tools are used: a quadruple Langmuir probe in vacuum and a fast camera installed outside the vacuum chamber. Among those diagnostics, the quadruple Langmuir probe is a reliable spontaneous measurement method for the measurements of electron temperature, density, and ion velocity, which are the plasma parameters should be known fundamentally for understanding the plasma jet. The fast camera imaging is also important diagnostic method to visualize the shape and motion of the plasma jet Therefore, two diagnostic tools are be used in combination in order to characterize the plasma jet. In parallel, an equivalent circuit simulation and the PIC (particle-in-cell) simulation for the rail gun plasma have been conducted to analyze the experimentally measured characteristics of the plasma jet more systematically.

1.2 Thesis outline

In the chapter 2, characteristic description and control method of ELM as background theory which are necessary for comparison with rail gun plasmas will be given. Also, rail gun dynamics will be introduced. In the chapter 3, experimental setup including rail gun and diagnostic tools will be introduced. In the chapter 4, diagnostics process for the rail gun plasmas will be discussed. Through the fast camera, the propagation of the plasma channel inside the rails is visualized with snap shots. Also, the plasma ejected from the rail gun is identified, and the plasma jet is measured by a quadruple Langmuir probe. The plasma jet parameters are calculated from the probe potentials and currents. Eventually, the plasma jet from the rail gun is proven to be useful to make ELM-like plasma, and the plasma parameters are compared with ELM filament plasma in terms of the particle and energy. In the chapter 5, it will be devoted to introduce theoretical models for rail gun plasma. The rail gun system is presented as simple circuit, and the plasma jet ejected from the rails is simulated by the particle simulation. The computational results are also compared with the experimental results. Finally, conclusions and future works in rail gun system will be described in the chapter 6.

Chapter 2 Background theory

2.1 Edge Localized mode (ELM)

Tokamak, one of fusion devices is important to drive stable H-mode in a long time. In order to maximize fusion power in next step device like ITER, operation in H-mode at possible pedestal pressure is needed. This is typically achieved in H-mode with type I ELM [11]. However, extrapolated to ITER collisionalities, the partial energy losses caused by type I ELM are incompatible with the life time of the divertor or plasma facing components [12]. Thus, understanding ELM physics and active control is crucial for ITER operation in future.

The ELM is a repetitive MHD instability due to a steep pressure or density gradient, which can generate at the edge boundary of the tokamak plasma in H-mode. Assuming that access to H-mode is achieved due to the high edge collsionality suppressing the bootstrap current, edge pressure could increase until the ballooning limit was reached. The growth of pressure pedestal stops at stable ballooning mode and then edge current rises due to the pedestal. After that, ELM crash occurs due to the increasing bootstrap current, and it is initiated the pressure gradient disruption at unstable bootstrap current. In this manner, ELM cycle that the pressure pedestal builds up and disrupts repetitively is formed typically.

The structure of ELM shows in Figure 2.1. Figure 2.1(a), the camera image of the ELM in MAST [13], presents that the shape of ELM is like filament. The nonlinear ballooning mode theory predicts that the mode will evolve into a filamentary structure, which is highly elongated along magnetic field lines shown in Figure 2.1(b). Each filament narrows and twists to push between filed lines on neighboring flux surfaces on the outboard side [14]. ELM plasma of highest stored energy in the filament is type I

ELM. It appears that the ELM repetition frequency ν_{ELM} increases with the energy flux through the separatrix,

$$\frac{d\nu_{ELM}}{dP_{sep}} > 0 . \tag{2.1}$$

Prior to type I ELM, the entire fluctuation level increases. During the type I ELM, there is a high level of incoherent magnetic fluctuations. In Eqs. (2.1), P_{sep} is the energy flux through the separatrix as following equation,

$$P_{sep} = P_{tot} - \frac{dW}{dt} - P_{rad} \tag{2.2}$$

where P_{tot} is total heating power, W is released energy and P_{rad} is radiated power [15].

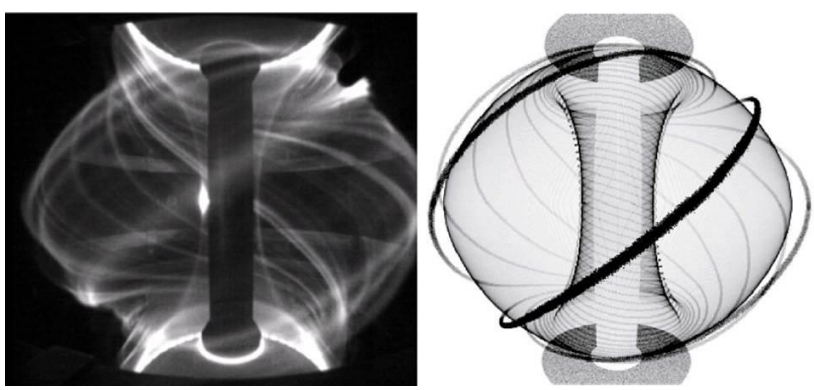

Figure 2.1 (a) Fast camera image of the ELM plasma obtained at the start of an ELM in MAST (left). (b) The predicted filament structure of an ELM in the MAST plasma geometry, based on the nonlinear ballooning mode theory (right). [13]

The high energy of type I ELM causes to decrease the lifetime of tokamak damaged in divertor or first wall. There are some control methods in order to prevent the effect of

ELM. One is called pellet pacing or pellet injection [9]. It is a control method of plasma frequency as the injection of fuel pellet. The injected pellet has so higher frequency than the ELM frequency that small ELM event is generated. The other ELM control method is RMP called resonant magnetic perturbation [10]. The RMP method makes to suppress the pressure gradient to prevent getting the limit of that in pedestal area as multiplying the isotropic plasma diffusion through the pedestal floor formed by magnetic field perturbation. Also, super-X divertor [16] and snowflake divertor [17] are controlling method for ELM plasma. Both divertors are an advanced concept that employs extreme manipulation of the diverted magnetic field in an effort to moderate the plasma conditions at the target. In addition, small and no ELM regimes [18] as well as active ELM control using ELM pace making by pellets and magnetic field perturbation, should be considered.

2.2 Rail gun dynamics

A rail gun is an electrically powered electromagnetic projectile launcher. The gun comprises a pair of parallel conducting rails along which a sliding armature is accelerated by the electromagnetic fields of a current that flows down one rail side, into the armature and then back along the other rail side [19] shown in Figure 2.2. Metallic sliding conductors are often the typical form of rail gun armature but plasma armature can also be used as a plasma gun. The plasma armature is formed by an arc plasma channel of ionized gas that is used to push a solid in a similar manner to the propellant gas pressure in a conventional gun.

In rail gun dynamics, the magnitude of the force called Lorentz force can be determined from a form of the Biot-Savart law. It can be shown from the Biot-Savart law that the magnetic field at a given distance from an infinite current carrying wire is given by

$$B(s) = \frac{\mu_0 I}{2\pi s} \tag{2.3}$$

where μ_0 is the permeability constant, I is the current flows through system, and s is the distance from an infinite current-carrying wire. It can be rewritten by

$$B(s) = \frac{\mu_0 I}{2\pi}\left(\frac{1}{s} + \frac{1}{d-s}\right) \tag{2.4}$$

where d is a rail separation distance which is in the space between two infinite wires. Assuming that the rail radius, r is very small compared with the rail separation distance and the rails are a pair of infinite conductors, the average magnetic field around a rail gun armature is expressed by

$$B_{avg} = \frac{\mu_0 I}{2\pi d}\ln\frac{d-r}{r} \approx \frac{\mu_0 I}{2\pi d}\ln\frac{d}{r}. \tag{2.5}$$

Finally, by Lorentz force, the magnetic force is given as follows,

$$F = IdB_{avg} = \frac{\mu_0 I^2}{2\pi} \ln \frac{d}{r}. \tag{2.6}$$

However, this equation is not easy to make an electromagnetic expression for the Lorentz force. In order to calculate the force reasonably, it is better that the rail gun system is assumed to an electric circuit. Under this assumption, the force, known as Lorentz force, becomes very large at high currents. It is expressed by

$$F = \frac{LI^2}{2} \tag{2.7}$$

where L is the inductance per unit length of the rails [20].

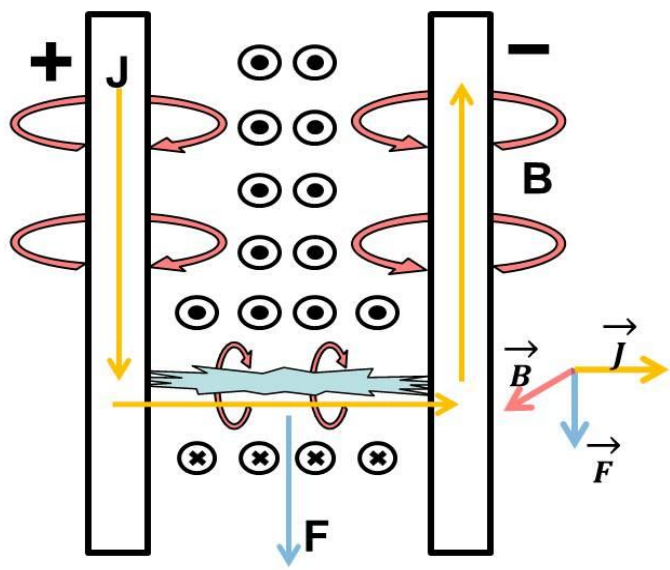

Figure 2.2 Conceptual schematic of principle rail gun dynamics.

Chapter 3 Experimental setup

3.1 Design requirements

Prior to design of the rail gun system for the ELM simulator, global ELM plasma parameters and requirements for simulating ELM filament plasma should be addressed. These parameters are listed in Table 3.1. In addition, it is required improvements based on the limitation of experimental results in previous rail gun design. These will be used not only for overall rail gun system design process in the next section, but also for installation of diagnostic tools such as fast camera and quadruple Langmuir probe and experimental conditions in the following sections.

The rail gun is required to make ELM-like plasma. Although the rail gun plasma temperature is difficult to reach to ELM plasma temperature without external heating, other parameters are confirmed the possibility to obtain though previous works. The ELM plasma density is $1\text{-}10\times10^{19}$ m^{-3} and the drift velocity is 10-15 km/s. The density can be obtained in arc plasma and the velocity is able to get through the acceleration in rail gun. For these purposes, the distance between rail gun electrodes and length of the rails are considered to rail gun system design. In addition, the rail gun is designed to prevent the puffing gas from being diffused out and to minimize the reduction of the lifetime of the rail gun due to the electrode dust.

Table 3.1 Main parameters of ELM filament plasma in ITER scale. [21, 22]

ELM parameter	**Type I ELM**
Energy Density	10 MJ/m^2
ELM Frequency	1-10 Hz
Total ELM duration	0.1-1 ms
Power Density	0.1-3 GW/m^2
$\Delta W_{ELM} / W_{pedestal}$	2-20 %
Pedestal energy	1-4 keV
Plasma Temperature	200-500 eV
Plasma Density	$1\text{-}10\times10^{19}$ m^{-3}
Plasma Velocity (AUG scale)	v_r = 1-3 km/s v_ϕ = 10-15 km/s
Spot size	δ_r = 7-10 cm $\delta_\perp$ = 23-30 cm

3.2 Construction of rail gun system

The overall rail gun system consists of three main parts. One part is power source including discharge switch for triggering and gas puffing device to feed argon or hydrogen gas. Another part is rail gun which is caused starting discharge and accelerating the plasma. Finally, the other is diagnostic part such as a fast camera and a probe to measure plasma generated from the rail gun. Figure 3.1 shows the picture of the overall experimental setup used in the present study.

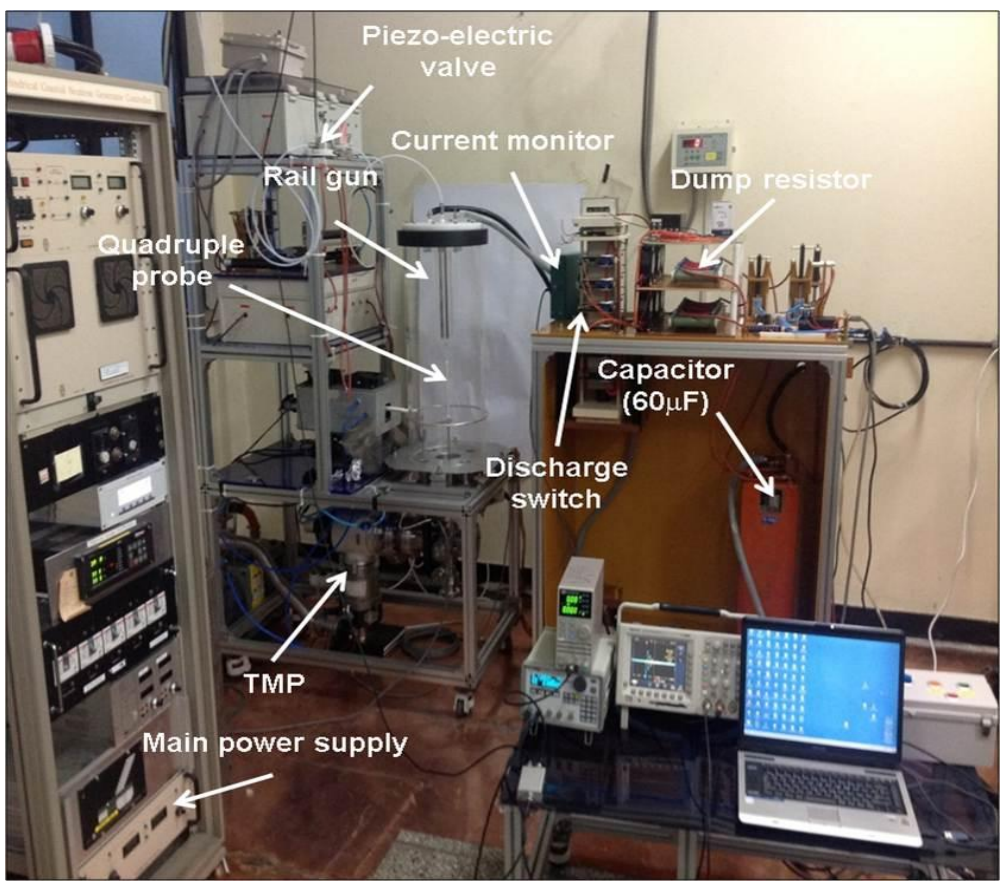

Figure 3.1 Photograph of overall rail gun system.

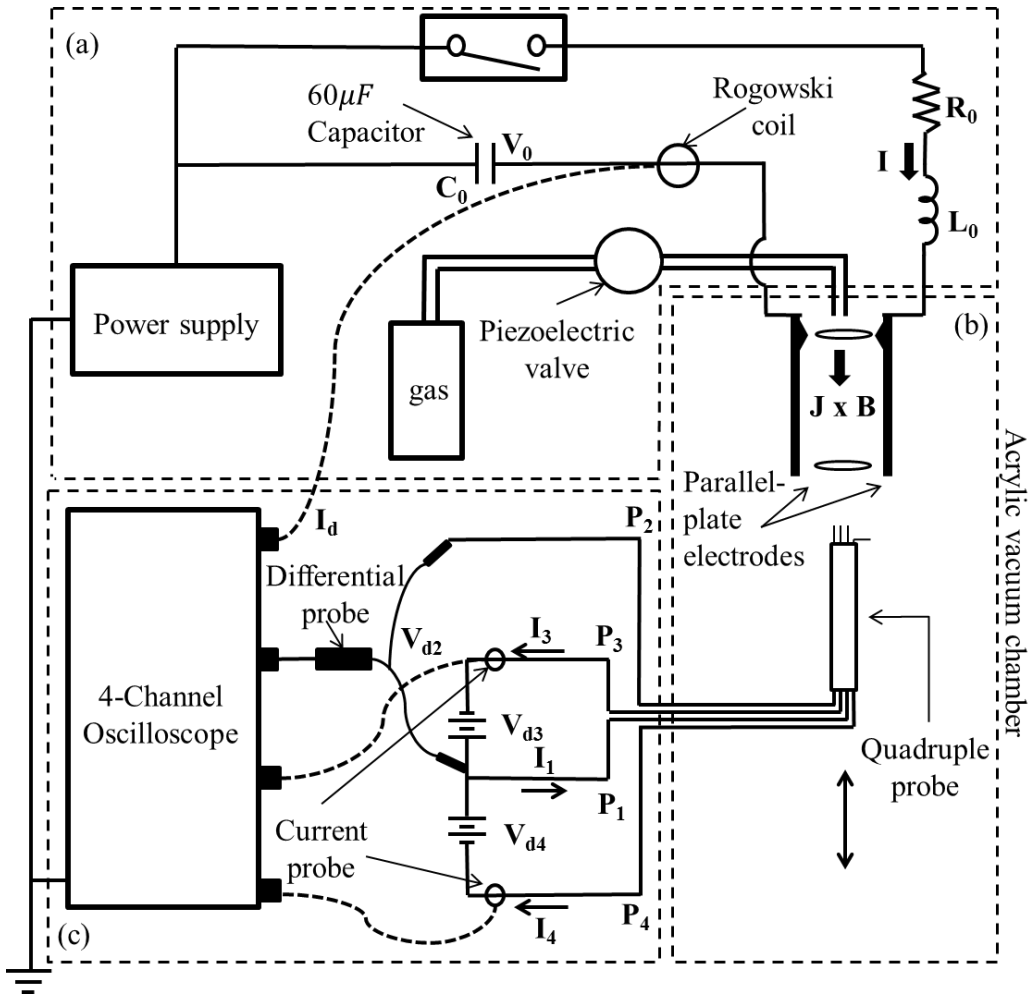

Figure 3.2 Schematic of the rail gun system. (a) Electronic diagram of rail gun, 3kJ pulse power source and gas puffing system. (b) Rail gun with two parallel-plate electrodes and vacuum chamber. (c) A quadruple Langmuir probe to measure characteristics of plasma jet and electric circuit for data acquisition.

3.2.1 Power supply and gas puffing system

Figure 3.2(a) shows the pulse power source with discharge switch and gas injection system. The power supply is capable to supply 10 kV with a 60 μF low inductance capacitor bank. The electrical energy stored in a high voltage capacitor is discharged to the parallel-plate rail gun by closing a main discharge switch and puffing of gas between two rails. The pulse switch (Astrol Electronic AG.) is possible to trigger until 15 kVdc, and its total pulse length is 10 μs with pulse frequency of 1 Hz. The gas is injected by a piezoelectric valve (Key High Vacuum Products. Inc., PEV-1) which is able to adjust the amount of gas depending on the preset voltage level.

In operation, puffing gas is used argon or hydrogen gas due to its well-known properties. The gas with constant 2 atm begins to be injected to the space between two rail electrodes in ignition starting time. The gas injection time is fixed to 10 ms. When the puffing time is too short, the discharge is not to start, while the arc plasma is not generated only once but several times in long injection time. The piezoelectric valve is opened as much as 80 % of total amount. The high current which flows through a discharge switch is supplied to rail electrodes during 8 ms after 31 ms from gas injection starting time, because the gas diffusing along the space between the rails takes the time to reach to discharge initiation point. This trigger delay time is important to trigger the discharge in proper time that the gas reaches to discharge starting point.

3.2.2 Rail gun design

The rail gun is established in vacuum chamber and the plasma coming out from it is diagnosed by a quadruple Langmuir probe shown in Figure 3.2(b). In this thesis, the design of rail gun was adopted for betiding plasma blob like ELM plasma. It was fabricated as a structure of the rail gun in a vacuum chamber in order to create plasma,

such as the ELM plasma. It is referred to as the plasma gun, because that generates plasma in vacuum environment.

Figure 3.3 shows a fundamental structure of the rail gun in acrylic vacuum chamber. Two stainless steel rails of 30 cm long, 1 cm wide, and 1 cm thick are assembled to be separated 1 cm each other. A gas puffing alumina tube fixed in polyacetal cap is set into the space between the rails. In order to produce the gas discharge in a constant position when gas is injected between the electrodes through the tube, each spine was welded on the electrodes shown in Figure 3.4. Figure 3.5 shows the sectional view of the rail gun structure. This view represents the design structure of the rail gun for the invisible part. The rails is fixed in the cap to prevent to widen by force to perpendicular to the rails.

It is necessary to collect the injection gas for discharge in order to make a plasma blob. For this purpose, four sides of two electrodes are enclosed by transparent acrylic plates, preventing the puffed gas to diffuse out the rail electrodes. The side walls are also used to support the rails against mechanical force during the discharge. The rails and side walls are designed to be apart from each other slightly to suppress unwanted surface discharge through coated conducting layers formed on both sides due to metal particles eroded from the rail surfaces. This is shown the transpicuous side walls to collect diffusion gas in Figure 3.6. For the above mentioned reason, there is a vacant space in acetal cap contact with the upper part of the electrodes. These are very important roles in the life of the plasma gun that is rail gun accelerating plasma in vacuum environment.

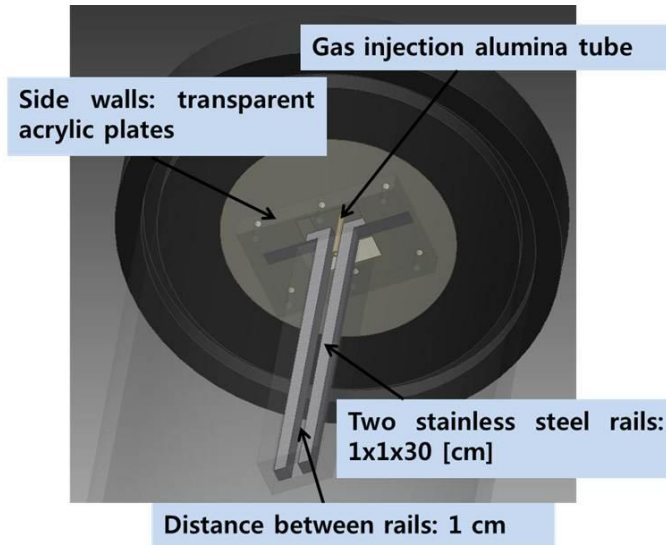

Figure 3.3 Structure of the rail gun : Two rail electrodes of the plasma gun, side walls surrounded the rails, a vacuum chamber.

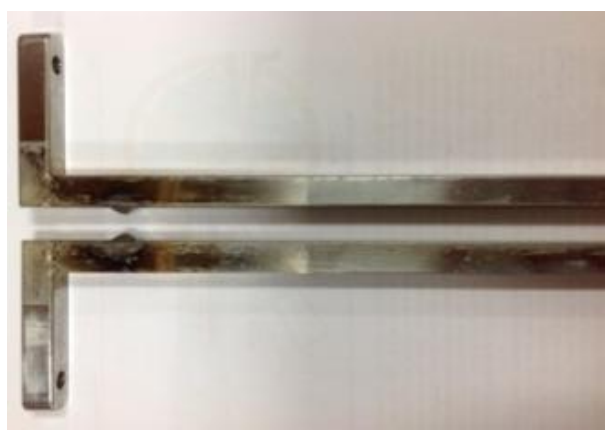

Figure 3.4 Spines welded on each rail for discharge in a constant position.

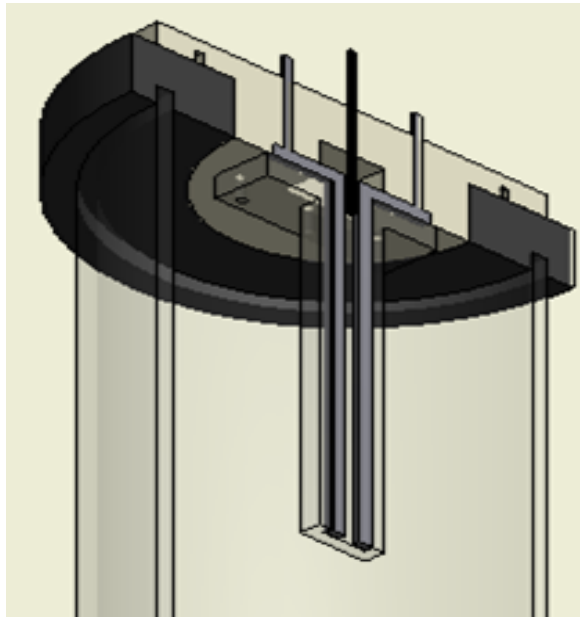

Figure 3.5 Sectional view of the rail gun structure.

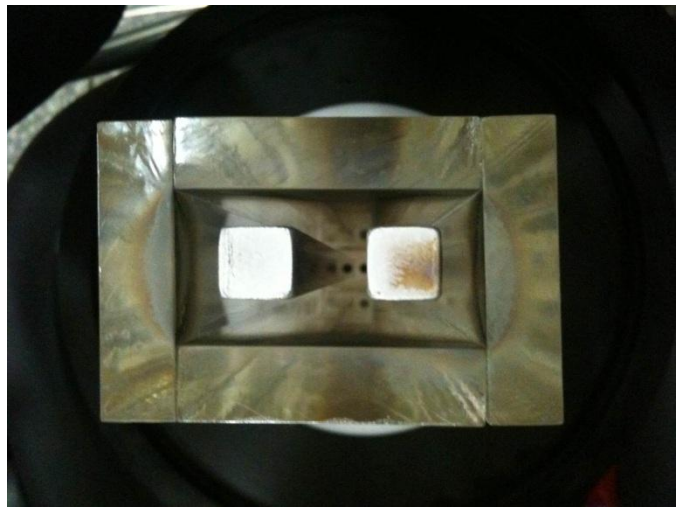

Figure 3.6 Transpicuous side walls to collect diffusion gas.

3.2.3 Installation of diagnostic tools

In this research, it is used two main diagnostic tools which are a fast camera and a quadruple Langmuir probe in order to measure plasma parameters. The fast camera is installed to look straight into the space between the two rails for imaging the arc plasma channel occurred in the space and the plasma jet launched out from it. In other words, it is observed dynamics of the arc plasma along the rails and characteristics like velocity of the plasma jet via the high speed camera. As a result, the images divided into two parts which are inside and outside of the rails show the characteristics of the rail gun plasma such as shape, position, and motion including the velocity.

A quadruple Langmuir probe as another diagnostic device is installed in vacuum chamber shown in Figure 3.2(b). It is standing along the propagation direction of the plasma jet. This probe is available to move 100 mm up and down with a linear feed-through (Huntington Mechanical Laboratories, Inc., L-2131-10-SF) which is used to work the linear motion in vacuum. The each tip of the probe is connected to the electric circuit in Figure 3.2(c) for signal processing, and a four channel oscilloscope acquires the electric signals.

The detailed specifications of the diagnostics tools such as a fast camera, a quadruple Langmuir probe and auxiliary devices is in the following section 3.3. And it also presents the experimental conditions and methods using the diagnostic equipment.

3.3 Diagnostics

3.3.1 Fast camera

In the rail gun, the arc plasma channel generated in the vicinity of the gas injection port is accelerated by well-known $J \times B$ force. And the plasma blob goes out from the plasma channel in the rails. Because its velocity is expected from a few km/s to hundreds of km/s, the high speed camera is essential to measure the fast plasma blobs indirectly as identifying the time and location of the plasma blob motion. Not only that, but it can be found the plasma shape in the rail gun.

The fast camera (NAC Inc., Megacam GX-8) has the following specifications. Its maximum shutter speed is 600,000 fps, and the resolution is available to 1280×1024 pixels. It is also possible to minimize the exposure time of 0.6 μs. However, it is required to find the proper values in this diagnostic, because it may not be obtained clear images in these specifications. After performing several pre-test, it was able to obtain the clear images in following conditions those are 250,000 fps, 16×64 pixels, and 0.8 μs in each spec. Note that the fast camera is located at distance approximately 5 m apart from the rail gun.

As mentioned in the previous section, the fast camera is looking at the two parts, the space between the rail and the outside of the rails. The camera images taken inside the rails are meaningful to estimate the change of the arc plasma channel velocity along the rails and the initial velocity spewing out of the rails according to the position over time. It also helps to identify the shape of the propagation of the plasma channel and the geometry of itself. On the other hand, the imaging focused on the below to the eruption part of plasma jet is to find out jet velocity depending on the time and location. In addition, it is possible to confirm that the plasma jet goes out of the electrodes while maintaining the form of a lump as well as the shape of itself can be observed.

3.3.2 Quadruple Langmuir Probe (QLP)

The quadruple Langmuir probe so called QLP is a diagnostic tool combined with triple Langmuir probe and crossed electrostatic probe. It is not required voltage sweep and complicated data processing, and instantaneously determines the values of the electron temperature (T_e), electron density (n_e), and ion velocity (v_i) [23]. These plasma parameters are important to define characteristics of ELM plasma. Especially, ion velocity is critical parameter in terms of the plasma particle control with certain external electromagnetic field. In general, it is impossible to measure the plasma velocity in the case of single Langmuir probe which is used most commonly. However, QLP is capable to measure the velocity with temperature and density at the same time. Thus, the QLP diagnostic is useful in ELM simulator which is important to compare with real ELM filament plasma characteristics and plasma jet parameters measured by diagnostic tools used in this research.

The QLP is made up as follows: 4 metal tips, ceramic rod, stainless steel rod and electric circuit for signal processing. Its 4 tips are constructed using tungsten wire of 0.3 mm in diameter. The length of each probe tip is 5.0 mm. The probe tips indicated as P_1, P_2, and P_3 in Figure 3.7(a) are parallel to the plasma jet direction, but P_4 is perpendicular to it, which is a conventional arrangement of the quadruple Langmuir probe. Each 4 tips are fixed on the ceramic rod, which has 4 holes. The ceramic rod is appropriate to plasma diagnostic due to the nonmetal material, but it is fragile. For these reasons, the ceramic rod was used to fix the each tip in plasma, and the part of rod that holds the probe was made by stainless steel shown in Figure 3.7(b).

Figure 3.7 Figuration of a fabricated Quadruple Langmuir probe. (a) Appearance of zoom in the end of QLP which has three tips parallel to plasma motion and one tip perpendicular to the motion. (b) overall structure of QLP.

This probe was connected to the electric circuit [24] for data processing. Figure 3.8 shows the electric circuit system fabricated to acquire electric signal. This is depicted by the electric circuit diagram in Figure 3.1(c) and 3.9. Two batteries of 9.4 V each are used to supply isolated voltage, V_{d3} and V_{d4}, to the probe tips. The collected ion currents, I_3 and I_4 by the probe tips are measured with the current probes (Pearson electronics Inc., 2878). The potential difference, V_{d2}, between P_1 and P_2 is obtained by a high voltage differential probe (Tektronix, P5205). The discharge current (I_d) between the electrodes is measured by a commercial Rogowski coil (Power Electronic Measurements Ltd., CWT 1500R) hanging on the line that connects between electrodes and a power source. The discharge current (I_d), potential difference (V_{d2}), and probe currents (I_3, I_4) are recorded to a four channel digital oscilloscope (Tektronix, DPO71040).

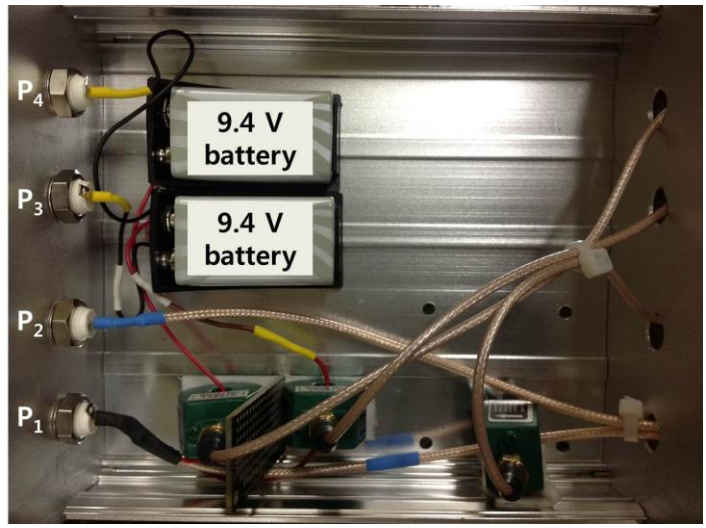

Figure 3.8 Electric circuit system for processing current signals collected by QLP.

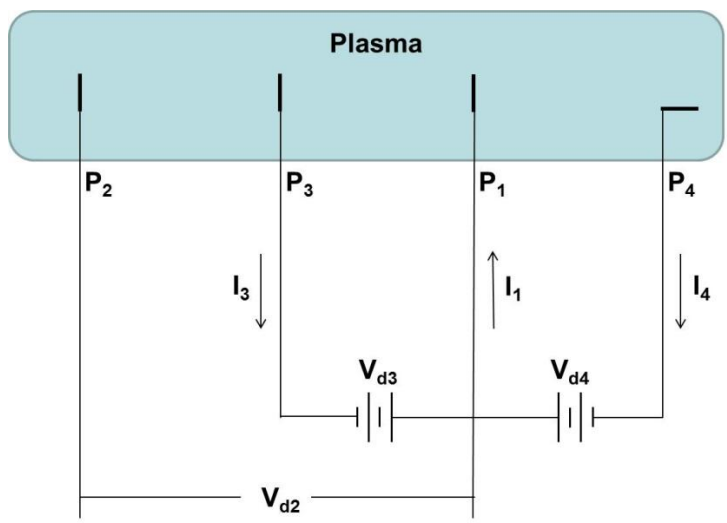

Figure 3.9 Schematic of the electric circuit for QLP.

Chapter 4 Characterization of plasma jet

A plasma jet is defined to the form of a lump launched from a part of the arc plasma channel which is reached to the end of the electrodes when it moves along the rails. This blob can be released from the end once or several times depending on the experimental conditions such as the charging voltage and the amount of the fuel gas. It is assumed that the size of the plasma jet is defined as at least a certain level of plasma density. In order to characterize the plasma jet, a fast camera and a QLP as diagnostic tools are employed. As a result, the characteristics of the plasma jet are found to be analogous with those of ELM plasma in some of the main features. The plasma jet is created by taking advantage of the rail gun as ELM plasma simulator, and then the ELM-like plasma form of a blob will be able to utilizing in aspects to particles control with external field or plasma facing component test using high energy in a laboratory environment.

4.1 Visualization of the rail gun plasma using fast camera

In general, the rail gun is capable to accelerate the armature so rapidly that it as the plasma accelerator is also expected to give the stronger Lorentz force to the plasma channel consists with ions, electrons, and neutrals of argon or hydrogen gas. Because of such a property, a fast camera may be useful to visualize the motion and shape of the fast plasma jet.

4.1.1 Arc plasma channel inside rail electrodes

Observing the inside of the rails is purpose to check the plasma channel accelerated down along the electrodes after the discharge in constant position and to estimate the initial velocity of a plasma jet tears from the channel. Images of the arc plasma channel

occurs inside the rails were taken by using a fast camera which is the state in focus on the internal electrodes entirely. Each image of the argon and hydrogen gas along the time variation is shown in Figure 4.1. The time interval for each image shot is 4 μs, and the images can be obtained in charging voltage of 2, 3 and 4 kV for argon and hydrogen. Each arc channel was started to form by the gas discharge in a constant position due to the protrusions on the rails. And then it was observed that the channel is accelerated down by the Lorentz force in each gas. In the case of argon, it takes about 28 μs that the plasma channel arrives the end of the electrodes after the initial discharge at charging voltage of 2 kV. And each arc channel reaches the end after around 20 μs and 16 μs at charging voltage of 3 kV and 4 kV. On the other hand, there is little difference in the time to reach by the degree of charging voltage in case of hydrogen, because the gas has so light mass and fast movement that the camera cannot take several shots accurately. For this reason, the argon gas is suitable in order to understand the shape of arc plasma and the initial velocity of plasma jet via snapshots of the fast camera.

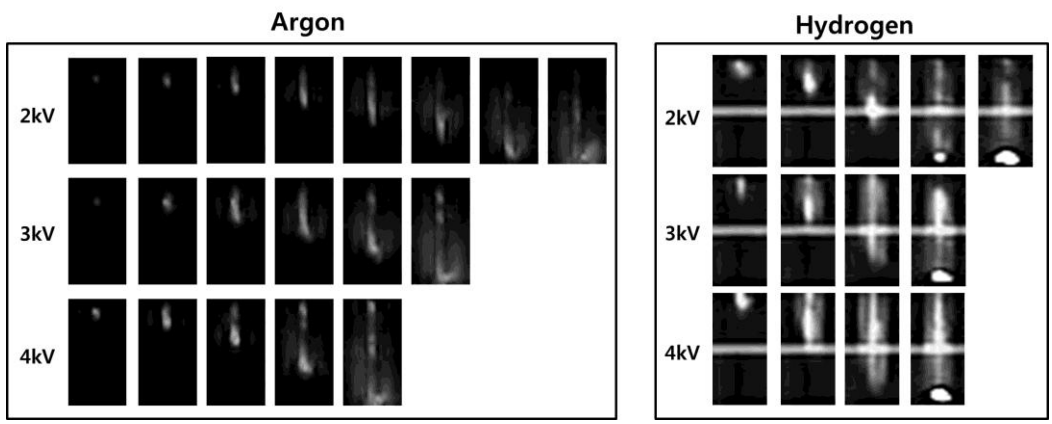

Figure 4.1 Comparison to images of the arc plasma channel accelerated in between the electrodes varying the time after the Ar and H_2 gas discharge.

In the snapshots of argon gas, the arc plasma channel is assumed to be a center of brightest point. Because the camera exposure time is 8 μs, it seems to like to be tail in given 4 μs per a shot. Under these assumptions, it can confirm that this plasma channel moves down along the rails. If the motion speed of the brightest point is considered the location-time dependency visually, the termination velocity of this channel is approximately more than 10 km/s at the end of rails in the case of each charging voltage. But this method might be inaccurate, because the images are confirmed with the naked eye and it can be ambiguous to assume the brightest point. So, this problem will be reliable with the rail gun modeling in in next chapter.

4.1.2 Plasma jet ejected from rail electrodes

In the previous section, the propagation of plasma channel within electrodes was observed in order to know its shape and velocity. As the following step, it have been explored the form of a plasma jet coming from charging plasma using a fast camera. For experiment, the camera focused empty space where from the half point of the electrodes to a QLP tip which is 132 mm away from the eruption part. As before, the time interval per a shot is 4 μs.

The results of the above experiment using hydrogen as puffing gas are shown in the following figure 4.2 and 4.3. Figure 4.2 shows the generation process of plasma jet ejected from squirt part. The plasma goes forward at the tip of rails, but it is difficult to determine the form of jet as a lump. Apparently, however, it can be confirmed that the plasma reaches the probe how to observe shining part around the probe into the plasma. This is clear basis to estimate that the plasma has reached on probe. When the stronger charging voltage of 3 kV is applied on the rails, the result is shown in following figure 4.3. The plasma is shown brightly due to more discharge caused by higher current, and it will move quickly. Likewise, the plasma reaches the probe instantly, but the path exists toward the side of probe. This minor problem is able to treat switching to dielectric

material from probe supporter, conducting material to stand the probe. It is still difficult to identify clearly the form of plasma jet as a lump and to determine the speed of that from single image which is from stating point to the probe, because the plasma is estimated about 10 km/s or more in Ar.

In next sections, it will be measure the velocity of plasma jet. Also, it will be compared with fast camera images and probe diagnostics. In addition, the investigation about the form of plasma jet will be made.

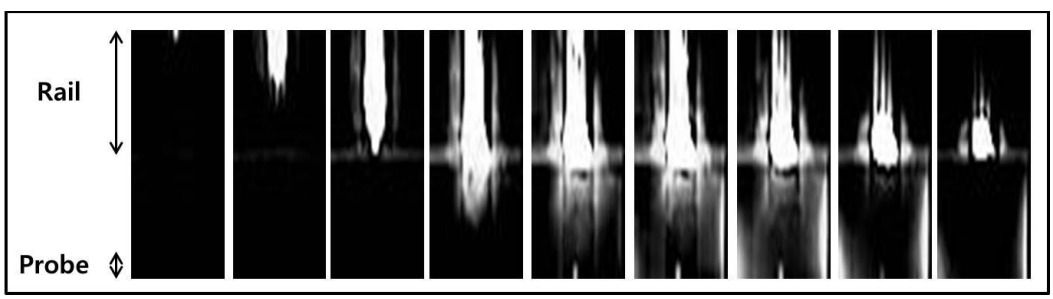

Figure 4.2 Generation process of the plasma jet ejected from the accelerated plasma channel at the charging voltage of 2 kV.

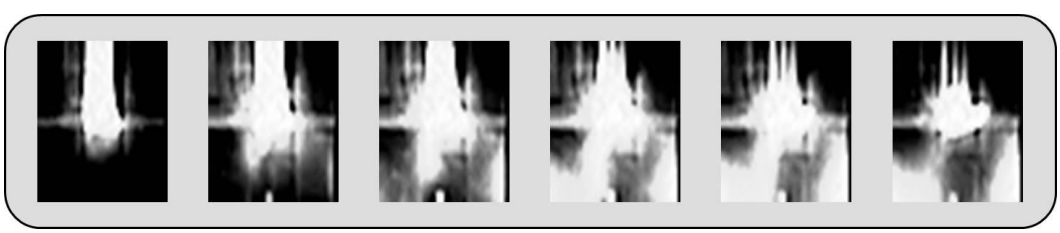

Figure 4.3 The plasma jet ejected from the accelerated plasma channel to the side of probe tip at the charging voltage of 3 kV.

4.2 Signal data acquisition using QLP

A QLP is used to measure the electron temperature, electron density, and ion velocity, while the probe is inserted into plasma. In this experiment, the QLP is applied to measure a fast plasma jet ejected from the rail gun in vacuum. The experiments are conducted at each charging voltage of 2 kV, 3 kV, and, 4 kV, and the probe is moved to be located at 52 mm, 72 mm, 92 mm, 112 mm in Ar gas and at 52 mm, 92 mm, 132 mm in H_2 gas from the exit of the rail gun.

Figure 4.4 shows the typical waveforms measured by the QLP as well as the discharge current waveforms and images of the time evolution of the position of plasma. In this case, the QLP is located at 52 mm apart from the exit of the rail gun at charging voltage of 2 kV. The meanings of each dot point in the figure are as follows.

- A: Discharge starting point
- B: Current collected point
- C: Exit of the rail gun (Peak discharge current 8~8.5 kA)
- D: Arrival time of the center of the jet to the probe position : ~25 μs
- E: Terminated point of the 1st plasma jet
- F: Termination of 2nd plasma jet

The discharge is stared in a constant location of the rails, and the plasma channel between the electrodes is accelerated along the rails due to $J \times B$ force with increasing current. The peak discharge current is measured to be 8~8.5 kA in this case, the discharge of 2 kV. At this time, most of the plasma reached the end of the electrodes. As can be seen from a point B, D, and E, the current is collected in the probe tips. The probe current I_3 and I_4 are observed to increase at approximately 25 μs, indicating the arrival time of the plasma jet to the measurement point of the probe. After this event, another plasma jet is ejected from rail gun shown in the interval, E-F. In general, the probe current is less than that of the first plasma jet at this time. Therefore it should be limited to focus only on the first plasma jet, since it is a target which is wanted to simulate ELM plasma.

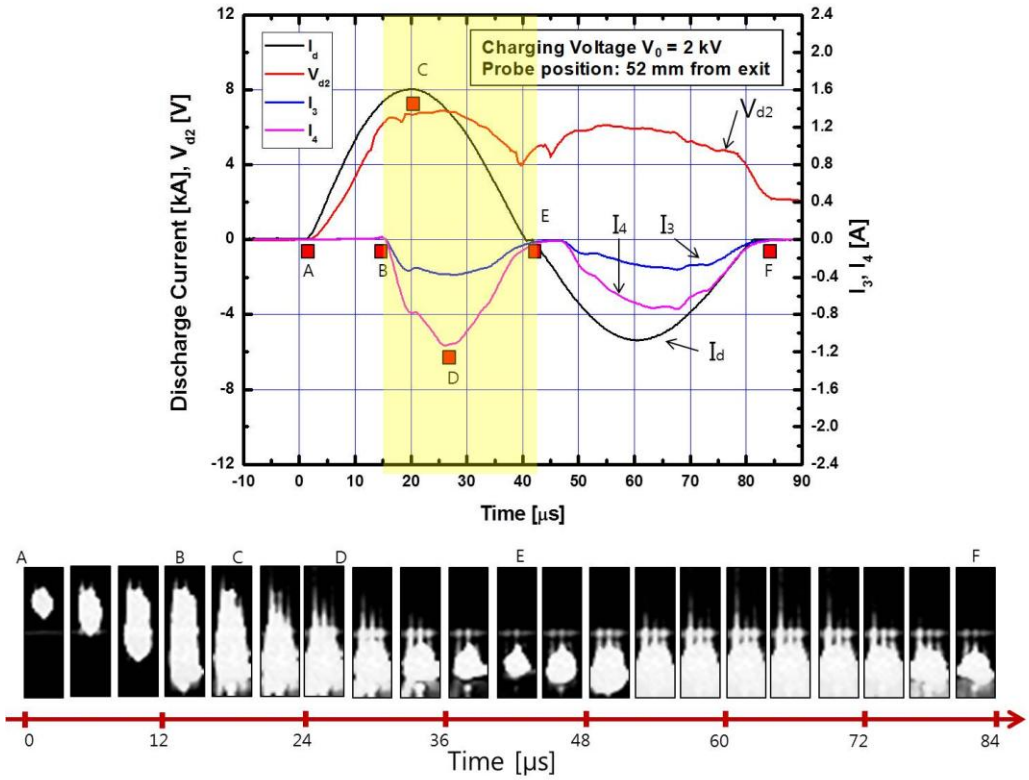

Figure 4.4 Discharge current (black), potential difference between P_1 and P_2 (red), and ion current collected by a probe parallel (blue) and perpendicular (pink) to the plasma velocity measured by QLP (top) and the time evolution of the position of plasma in overall rail gun system (bottom).

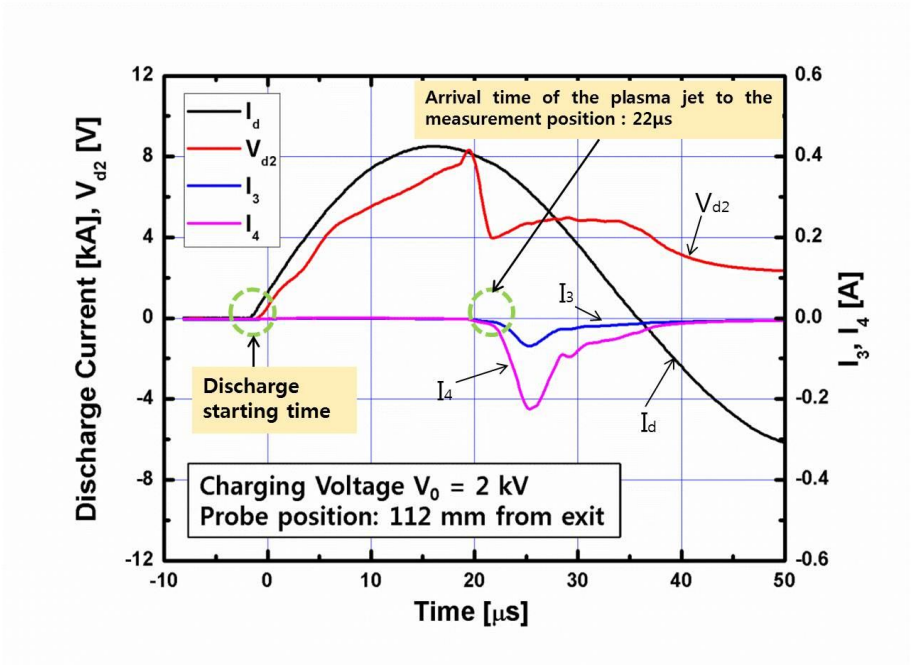

Figure 4.5 Discharge current (black), potential difference between P_1 and P_2 (red), and ion current collected by a probe parallel (blue) and perpendicular (pink) to the plasma velocity in first Ar plasma jet.

The plasma jet is ejected from the rail gun in about 3~4 times. The number of the plasma jet is related to period of the discharge current. In general experimental results, one plasma jet is generated in the half-period of the discharge current. The half-period is about 40~45 μs. The experimental result for first Ar plasma jet is shown in Figure 4.5.

4.3 Plasma jet parameters

4.3.1 Calculation of plasma parameters

In order to obtain the plasma parameters, the experimental results of the probe measurement should be calculated in equations for analyzing QLP data. The plasma parameters, T_e, n_e, and v_i, are determined from I_d, V_{d2}, I_3, and I_4 measured by QLP. For $V_{d3} = V_{d4} = 9.4V$, the electron temperature is dominant to V_{d2} in following equation [25],

$$1 = \frac{1 + \exp(\phi V_{d3}) - 2\exp[\phi(V_{d3} - V_{d2})]}{(I_4 / I_3)\{\exp[\phi(V_{d3} - V_{d2})] - 1\}}. \tag{4.1}$$

It is determined in Eqs. (4.1), where ϕ is e/kT_e. Note that e is electric charge and k is Boltzmann's constant.

For $A = A_1 = A_2 = A_3$, the ion saturation current density j_i is depended on measured values by [25],

$$j_i = \frac{(I_3 / A_3)(1 + I_4 / I_3)}{\exp(\phi V_{d2}) - 1} \tag{4.2}$$

where A is the collective area of the probe tip. For a plasma with only ion mass m_i, the Bohm sheath analysis which is relating j_i to the electron density gives,

$$j_i = en_e \left(\frac{kT_e}{m_i}\right)^{\frac{1}{2}} \exp\left(-\frac{1}{2}\right). \tag{4.3}$$

The electron density is easily obtained by combining Eqs. (4.2) and (4.3),

$$n_e = \frac{(I_3 + I_4)\exp\left(\frac{1}{2}\right)}{A_3 e\left(\frac{kT_e}{m_i}\right)^{1/2}\left[\exp(\phi V_{d2}) - 1\right]}. \tag{4.4}$$

For P_3 and P_4, $I_\perp$ is ion current collected by a probe perpendicular to the plasma velocity, I_4, and $I_\parallel$ is ion current collected by a probe parallel to the plasma velocity, I_3. For maxwellian electron and ion velocity distributions, the ion current ratio is [26],

$$\frac{I_\perp}{I_\parallel} = \frac{2}{\sqrt{\pi}}\exp\left[-\left(\frac{v_i}{c_m}\right)^2\right]\sum_{n=0}^{\infty}\left[\frac{(v_i/c_m)^n}{n!}\right]^2\Gamma\left(n+\frac{3}{2}\right) \tag{4.5}$$

where c_m is the most probable thermal speed of ions,

$$c_m = \sqrt{\frac{2kT}{m_i}}. \tag{4.6}$$

And Γ is gamma function,

$$\Gamma(z) = \int_0^\infty t^{z-1}e^{-t}dt \tag{4.7}$$

that is known as the Euler integral where the notation $\Gamma(z)$ is due to Legendre and z is the real part of the complex number.

In this manner, each plasma parameters which are T_e, n_e, and v_i, can be taken to solve the nonlinear equations (4.1), (4.4), and (4.5). In the results of above equations, the electron temperature is dominated potential difference between P_1 and P_2, and the electron density is proportional to total ion currents. Also, ion velocity is related to a constant that is ion current ratio of I_4 to I_3.

4.3.2 Time varying plasma jet

Through calculation for non-linear equations in previous section, the temporal plasma parameters which are election temperature, electron density, and ion velocity are gained in a specific probe positions. The plasma jet parameters of argon gas varying time in a location are shown in Figure 4.6. In the case of Ar gas, each peak value is obviously represented in the electron density. It is assumed that the peak points are a center of the plasma jet. The peak density is measured to be approximately 3×10^{19} m^{-3} at a probe location of 112 mm apart from exit. And each electron temperature and ion velocity is almost constant as around 3 eV and approximately 11 km/s at the time of peak density. When the plasma jet passes in a fixed measurement point of the probe, the plasma density increases sharply in the time of 20~25 μs after the ignition. The plasma velocity remains constant value in time interval of the density of more than about 1×10^{19} m^{-3}, and then it reduces drastically in the moment that the density is less than about 1×10^{19} m^{-3}. Unlike other plasma parameters, the electron temperature almost does not change with time. As well as the other probe location, the results show similar type of wave form temporally, but the temperature and density of the electron tend to decrease in farther probe location.

It is meaningful in the time intervals that the electron density is greater than about 1×10^{19} m^{-3} considering that the speed of the plasma jet maintains in the intervals, and ELM plasma density in the actual tokamak is more than approximately 1×10^{19} m^{-3}. Therefore, the plasma over the certain density in the time interval can be limited to the plasma jet. As shown in Figure 4.7, the time segment which is from 23 μs to 31 μs can be defined as a size of the plasma jet. The size is a length of jet toward a probe. The length in the flow direction of the jet can be estimated as roughly 8 cm at measurement position, since it moves the average velocity of 11 km/s in 7~8 μs. In this way, the length of the plasma jet ejected from rail gun is defined in each case. Note that the size of the plasma jet is the important parameters to investigate the effectiveness of plasma particle control carried out in the future experiment.

Figure 4.8 shows the plasma jet parameters varying time in each location, when the hydrogen gas is supplied for discharge. These results do not to emerge peak plasma density clearly depending on the time unlike Ar plasma density. It is assumed that plasma jet is one point in order to know the plasma parameter at the peak velocity, highest kinetic energy. The each peak velocity is measured to be approximately average 120 km/s, 140 km/s, and 160 km/s at a probe location of 132 mm apart from exit. The each electron temperature is around 9 eV, 10 eV, and 14 eV at the times in their peak velocities. Likewise, the each electron density is about 1×10^{19} m^{-3}, 1.5×10^{19} m^{-3}, and 5×10^{19} m^{-3} at that time.

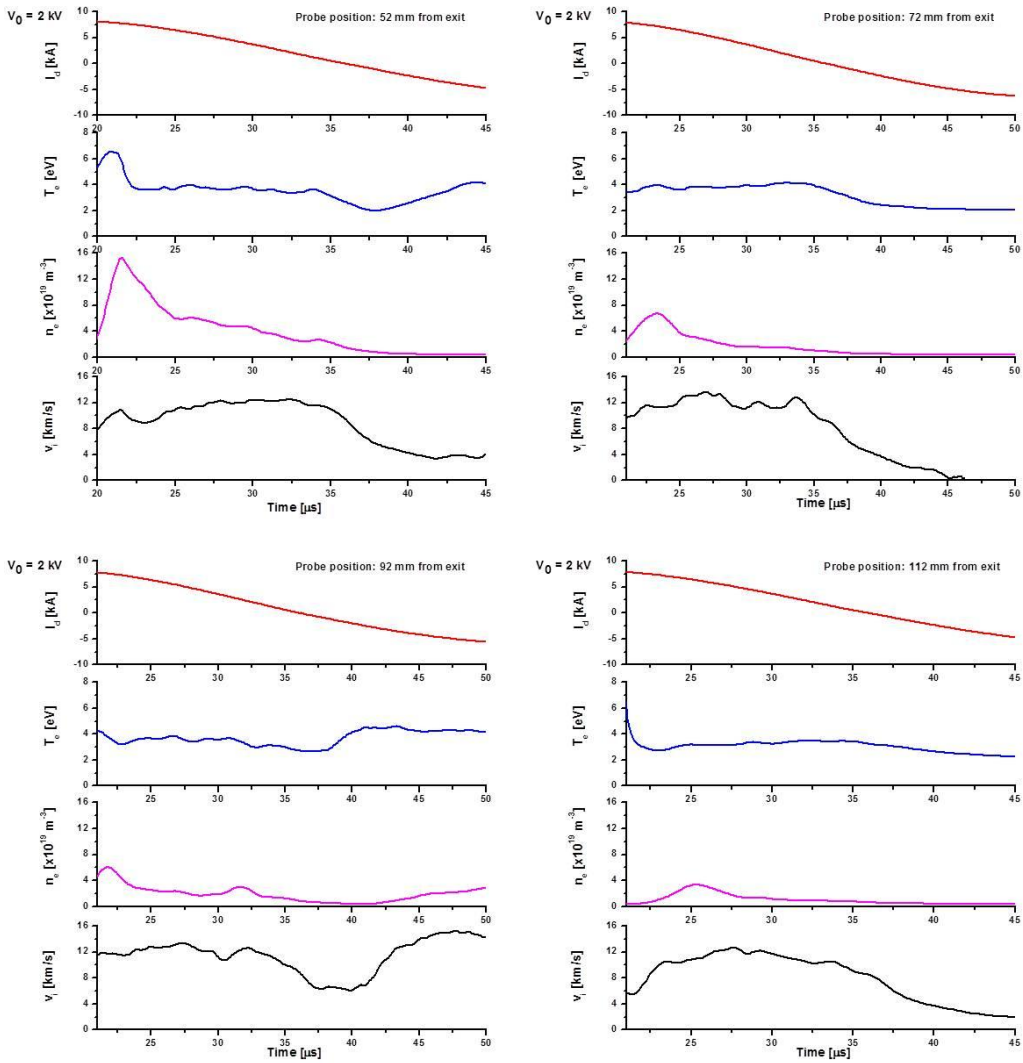

Figure 4.6 Discharge current (red), electron temperature (blue), electron density (pink), and ion velocity (black). Temporal Ar plasma parameters are calculated by the measurement data from the time of ~20μs after ignition. At charging voltage of 2 kV, the measurements were conducted in the location of each 52 mm, 72 mm, 92 mm, 112 mm.

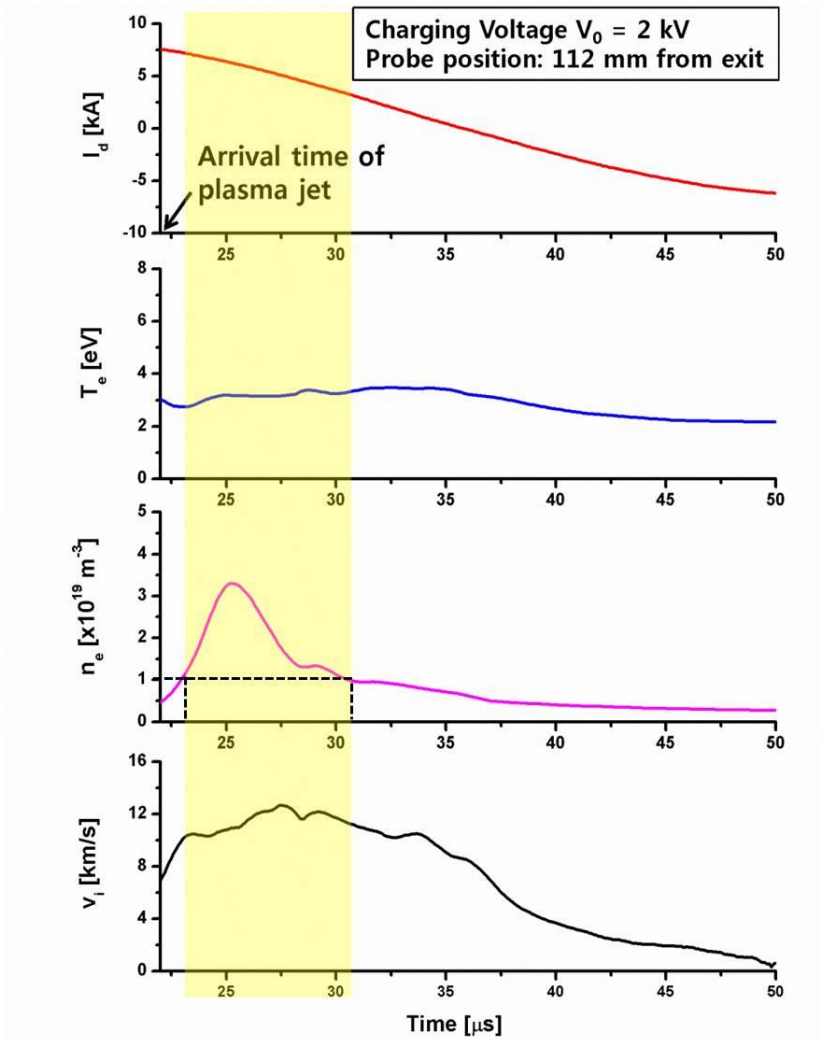

Figure 4.7 Decision criterion for the scope of plasma jet size using temporal plasma parameters. Discharge current (red), electron temperature (blue), electron density (pink), and ion velocity (black).

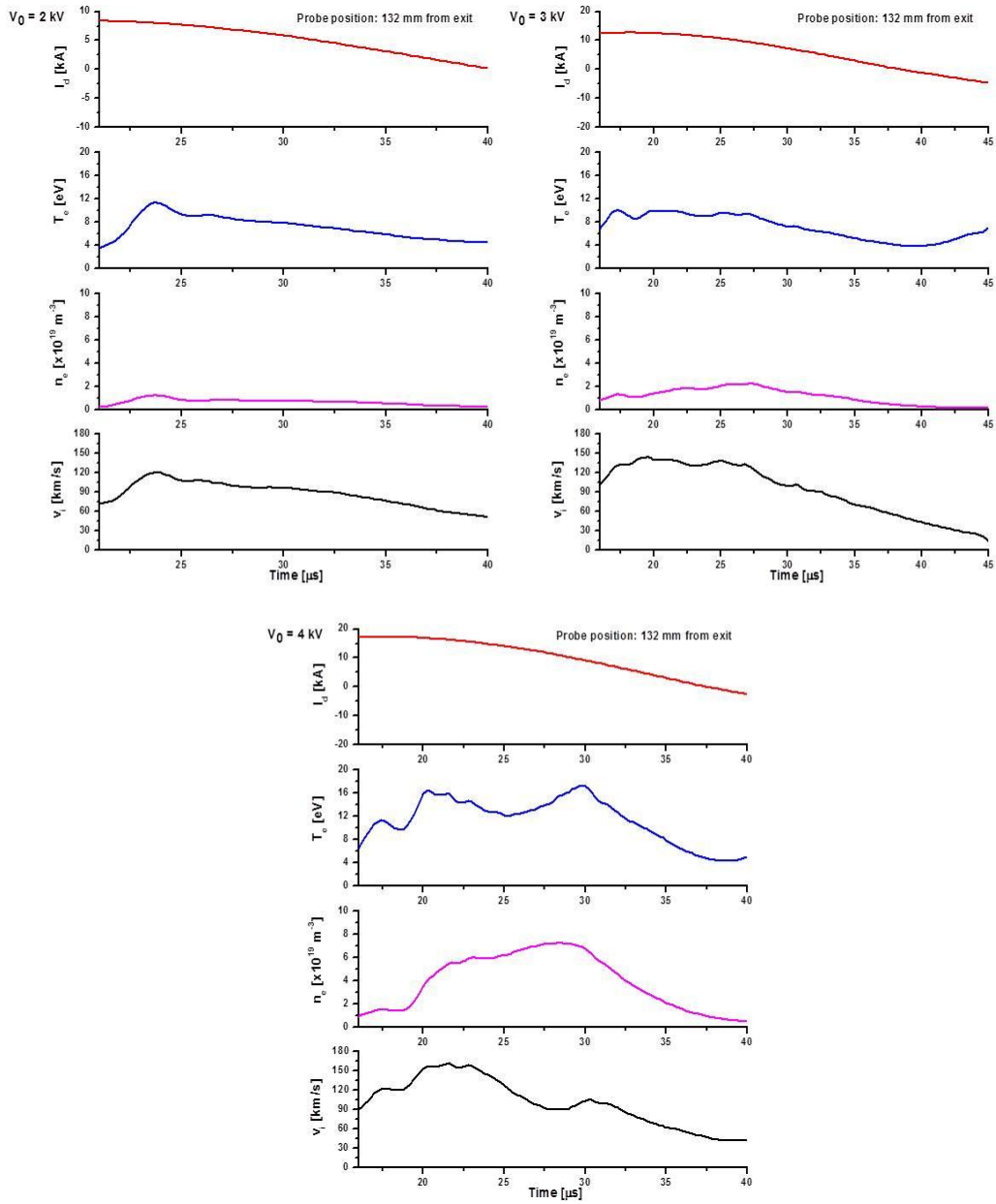

Figure 4.8 Discharge current (red), electron temperature (blue), electron density (pink), and ion velocity (black). Temporal H plasma parameters are calculated by the measurement data from the time of ~20μs after ignition. At charging voltage of 2 kV, 3 kV, and 4 kV, the measurements were conducted in a probe position.

4.3.3 Variation of moving plasma jet characteristics

It is expected that a plasma jet propagates in free space while the specific form is maintaining after outburst from the rail gun. However, the plasma parameters could be confirm to exist across the wide time zone from the results that the characteristics of the time varying plasma jet are measured by the QLP in a certain location. In other words, it does not maintain the form of a lump completely, spreading in the vacuum space. Therefore, it is necessary to diagnose the spatial change of the plasma jet, while changing the measurement location of the probe. The results are shown in Figure 4.9 and 4.10.

The spatial variation of the plasma jet is traced by changing the probe position at the same experimental condition. As shown in Figure 4.9, the ion velocity is almost not changed. The nearly constant ion flow velocity is attributed to low background pressure. Therefore, the ions are considered to be non-collision, and it moves constantly with the inertia. However, the electron temperature and density are observed to decrease continuously with distance from exit. Likewise, this tendency is not change largely at different charging voltage of 3 kV and 4 kV shown in Figure 4.10.

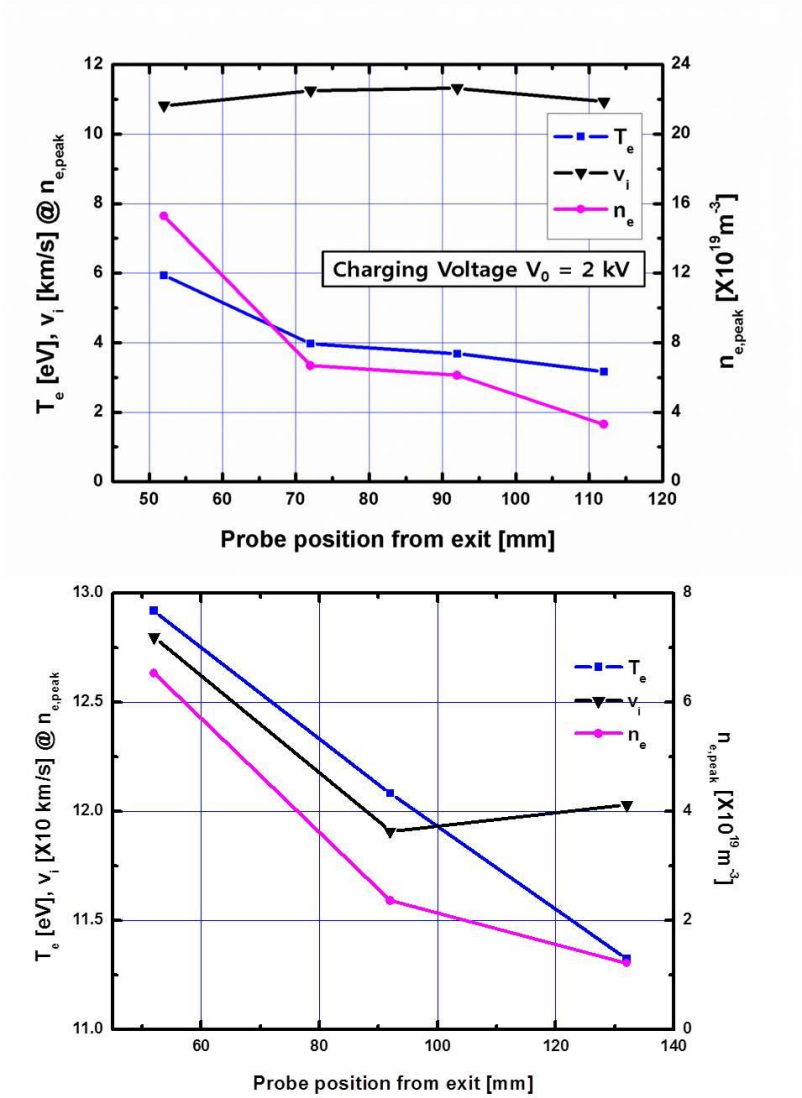

Figure 4.9 Variations of electron temperature (black), electron density (pink), and ion velocity (black) of Ar (top) and H (bottom) plasma measured depending on the probe positions. 52 mm, 72 mm, 92 mm, and 112 mm from exit at 2 kV charging voltage and peak electron density (top), 52 mm, 92 mm, and 132 mm from exit at 2 kV charging voltage and peak ion velocity (bottom).

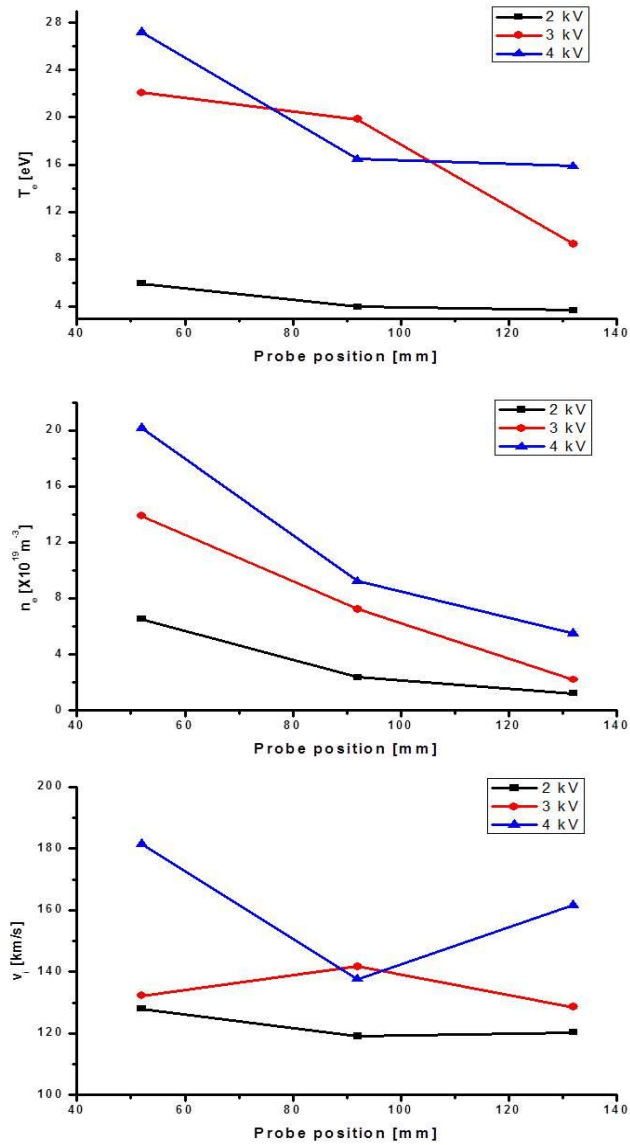

Figure 4.10 Variations of electron temperature (top), electron density (middle), and ion velocity (bottom) of H plasma measured depending on the probe positions, 52 mm, 92 mm, and 132 mm from exit at charging voltage of 2 kV, 3kV, and 4 kV.

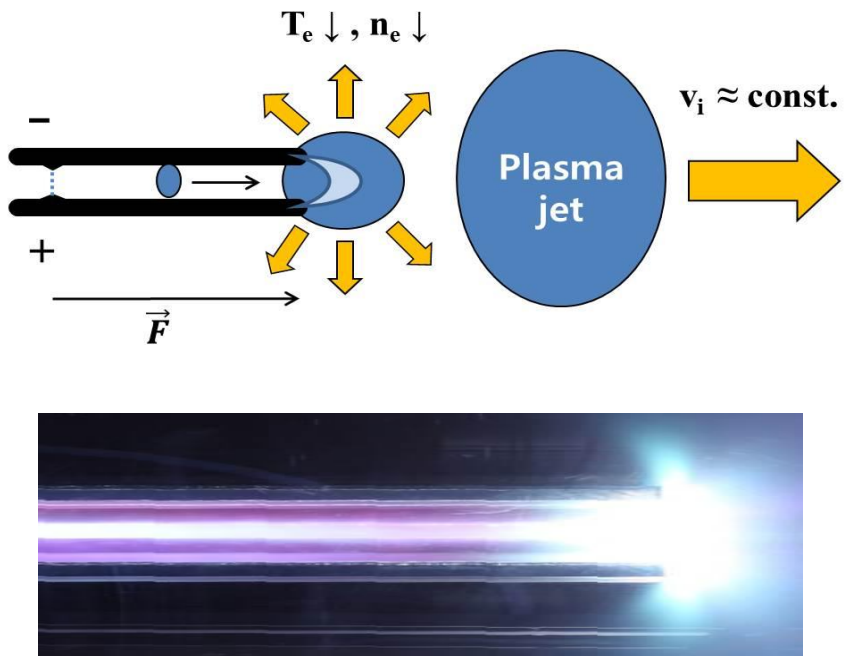

Figure 4.11 (a) Schematic drawing of the plasma jet diffusion. (b) Photograph of the plasma jet that is ejected from the electrodes.

Figure 4.11 shows that the plasma temperature and density tend to be affected due to diffusion of the plasma jet. The velocity is almost constant in same condition. In other words, the parameters except of the ion velocity decrease gradually, because of the broaden particle distribution the plasma jet is spread continuously during its linear motion. The velocity is irrelevant virtually with the particle diffusion. The origin of the plasma velocity is Lorentz force which is proportional to the current in rail gun, and the velocity due to the force is very fast relative to the diffusion rate. In addition, it should be careful that the size of first plasma jet is defined to not entire diffused bulk plasma, but the plasma chunk which is the density of more than 1×10^{19} m^{-3}.

4.4 Correlation of the ELM plasma and experimental results

4.4.1 Analysis as the particle

In this study, it is the ultimate objective to characterize the plasma jet made from the plasma gun in order to challenge controlling the ELM-like plasma in a laboratory environment. Actual ELM plasma can be compared with the plasma jet parameters obtained from the above experiments. The experimental plasma jet parameters are shown in following Table 4.1.

Table 4.1 Ar plasma jet parameters at charging voltage of 2 kV.

Plasma jet parameter	Probe position from exit			
	52 mm	72 mm	92 mm	112 mm
Electron temperature [eV]	6.5	4	3.5	3
Electron density [m^{-3}]	15	7	5.5	3.5
Ion velocity [km/s]	11	11	12	11
Spot length [cm]	19	17	16	8

Actually, the ELM plasma characteristics are not yet disclosed clearly in ITER scale. However, there have been progressed the studies about spatial and temporal evolution of the ELM filamentary structure and plasma characteristics such as temperature, density, velocity, and size in the ASDEX Upgrade [27], MAST [28], JT-60U [29] tokamak. Especially, it was carried out a variety of experiments to investigate ELM plasma parameters in ASDEX Upgrade and MAST. Understanding the temperature, density, velocity, and size of the ELM filament in general tokamaks or ITER is crucial to compare with the rail gun plasma in order to utilize as ELM-like plasma in small device. The

following paragraph describes the type I ELM plasma parameters in ASDEX Upgrade and MAST.

The measured average ELM filament plasma particle ion temperature is in the range of 50~80 eV in the far SOL (separatrix distance > 40 mm). The ion temperature (T_i) [27] or ion thermal energy as derived from the measurement is about a factor of ten below the pedestal ion energy of about 800 eV. The plasma density (n) is approximately $3\sim6\times10^{19}$ m^{-3} in the filament at a separatrix distance of 40 mm which is about the pedestal density [30]. The plasma velocity as most important plasma parameters is considered as the speed of the two directions. One is a mean radial (v_r) velocity [31] obtained of 1~9 km/s, and the radial velocity is of the ELM filament is represented as a function of distance from the LCFS. Another is a toroidal (v_ϕ) velocity [28] which decreases from approximately 15 to 2 km/s while the radial velocity increases from 1 to 9 km/s. In addition, the size is critical plasma parameter in aspect to analysis of the particle for plasma control. Each perpendicular ($\delta_\perp$) and radial (δ_r) size [32] of the filaments as a function of tokamak minor radius is 8~13 cm and 1~5 cm estimated by the combination with the velocities and measurements of the temporal width and separation of peak values observed in ion saturation current traces during ELM on the machines.

The results from small tokamaks could be converted to estimate on ITER scale [33]. There is, however, theoretical limitation to estimate the ELM plasma parameters such as the velocity on ITER modeling [34]. Therefore, it had to be done the quantitative parameters comparison of rail gun plasma characteristics in this experiment and results in existing devices, not ITER reference scenario.

The plasma density, velocity, and size are more important than the plasma temperature called thermal energy in aspect to control the particles with external electromagnetic fields. These results from Ar plasma jet shows that although the electron temperature of the plasma jet is less as much ~1/10 as it of ELM plasma, the electron density of the plasma jet is turned to be similar to ELM, assuming $T_e=T_i$ and $n_e=n_i$. And the spot size is similar level compared to ELM plasma in terms of the width and length.

Furthermore, the rail gun plasma velocity of ~11 km/s is analogous to the toroidal transport of ELM plasma in ASDEX Upgrade. Therefore, the rail gun plasma will be used in the experiment to control ELM-like plasma with external electromagnetic fields prior to reaching in the target.

4.4.2 Analysis as the energy

Thermal heat loads to the first wall and divertor during ELM have been known as one of the critical issues for ITER burning plasma operation. These heat loads with the energies transported by ELM ions toward the first wall, which depend on dissipation by parallel losses of the ELM energy to the divertor targets as the ELM particles travel across the SOL [30]. In order to the heat load test, the conventional plasma guns or accelerators have been used to make high heat flux and power. There are, however, drawbacks that the devices have complex structure and low cost efficiency. The rail gun had simple structure relative to the existing devices is able to produce faster particles as well as ELM-like plasma. Unwillingly, the kinetic energy of fast particles means that it may be equivalent of thermal energy, heat flux.

Figure 4.12 shows the comparison between the calculated kinetic energy from results of the ion velocities of H and the impact energy levels of the ELM plasmas in ASDEX Upgrade, JET, and ITER. Each impact energy in AUG and JET is 160 eV and 400 eV [30], and it is estimated of 1 keV in ITER scale [33]. In Table 4.2 from results of H plasma parameters, their velocities are similar level to the impact energy of ASDEX Upgrade. If the charging voltage increases to raise the current flows in rails, it will be able to get the effect of higher impact energy due to the increase of the particle velocity in the rail gun. Therefore, the rail gun plasma generated by puffed hydrogen also available as a substantial high heat flux device in order to test plasma facing components.

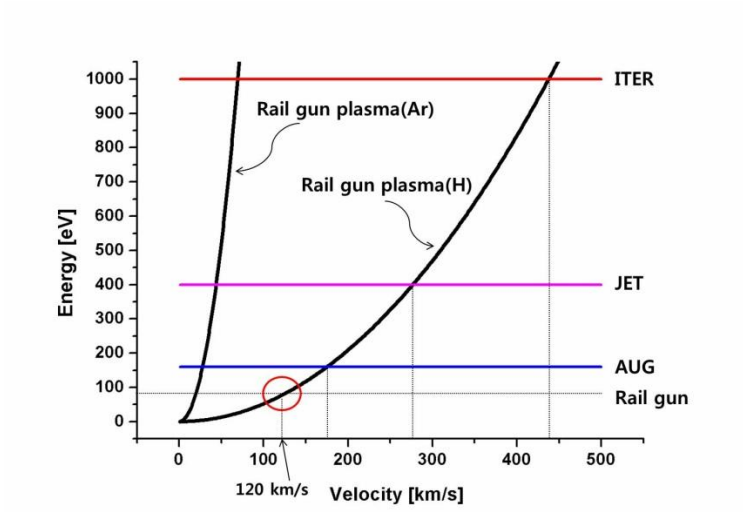

Figure 4.12 Conversion of kinetic energy-velocity of rail gun plasma jet and impact energy of the ELM filament in ASDEX Upgrade, JET, and ITER.

Table 4.2 H plasma jet parameters varying charging voltage and probe position.

Charging voltage [kV]	Probe position [mm]	Plasma parameters		
		T_e	n_e	v_i
2	52	12.8	6.5	127
	92	11.3	2.2	115
	132	10.7	1.1	117
3	52	20.7	13.3	126
	92	17.4	6.6	149
	132	9.3	2.1	131
4	52	26.3	20	180
	92	15.7	9.1	132
	132	14.4	6.4	122

Chapter 5 Theoretical models for rail gun plasma

A theoretical slug model and the PIC (particle-in-cell) simulation for rail gun plasma are developed. In the slug model of the rail gun electrodes, the primary concept of this simple slug model mainly originates from modeling with the consideration of the full electrical circuit. The circuit equation, therefore, which indicates the current, is chiefly derived from the Kirchhoff equation. Besides, this equation is coupled to the equation for the conservation of energy. On the other hands, the PIC simulation is carried out in order to identify the motion of plasma jet ejected from electrodes. Consequently, the models are verified by the comparison between numerical results and experimental data.

5.1 Theoretical slug model for the plasma gun

5.1.1 Simple system circuit model

The rail gun system including a capacitor, electrodes, and the electric lines connecting them can be represented as a simple electric circuit [35]. The equivalent rail gun circuit is shown in Figure 5.1. It is assumed that the radiation energy of the arc plasma channel is neglected and the plasma sheath is a good conductor [36]. It is also assumed that the resistance and inductance of the plasma channel due to the discharge is neglected. Kirchhoff equation for rail gun circuit is shown in following Eqs. (5.1),

$$\frac{d}{dt}\left(L_0 I(t)+\Phi\right)+\left(R_0+2R_1 x+R_p\right)I(t)+\frac{Q}{C_0}=V_0 \tag{5.1}$$

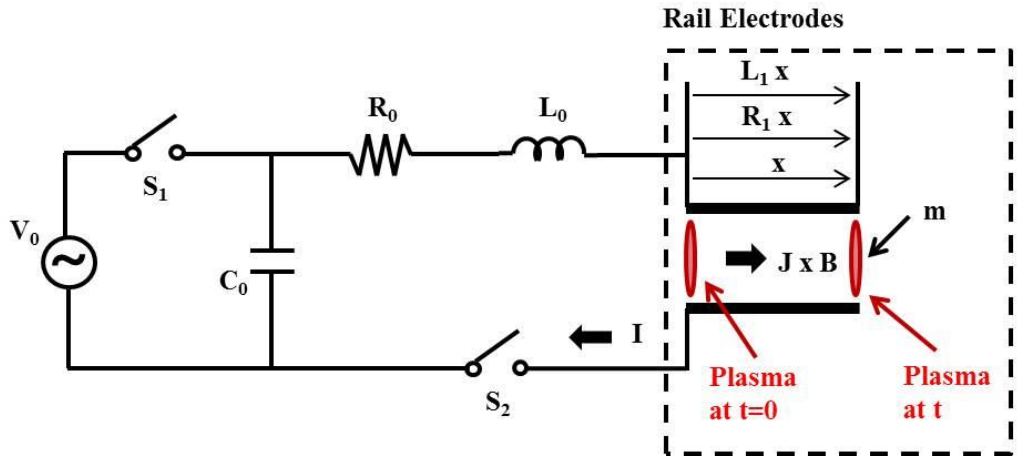

Figure 5.1 The equivalent circuit model for a parallel plate rail gun.

where L_0 is the inductance of discharge circuit, not including inductance of the rails, I is circuit current depending on the time, R_0 is the resistance of the circuit, R_1 is the internal rail resistance per unit length in the x, total length of the rail, R_p is the resistance in plasma channel, Q is the instantaneous charge on the capacitor bank of C_0, and V_0 is charging voltage. With these assumptions, Kirchhoff equation in Eqs. (5.1) for the rail gun circuit may be written as

$$\left(L_0 + L_1 x\right)\frac{dI(t)}{dt} + \left(R_0 + 2R_1 x\right)I(t) + \frac{1}{C_0}\int_0^t I(\tau)d\tau = V_0 \tag{5.2}$$

where L_1 is the internal rail inductance per unit length, and the magnetic flux between the rails, Φ is given by

$$\Phi = \left(L_1 x + L_p\right)I(t). \tag{5.3}$$

The equation of motion for the plasma channel can be expressed by

$$F = m\frac{d^2x}{dt^2} = \frac{L_1}{2}I^2 \tag{5.4}$$

where F is force by magnetic field in inductor, and m is the mass of the plasma channel, in terms of position of the plasma channel and the current flows in the plasma. Eqs. (5.2) and (5.4) are coupled and calculated in order to estimate the position of the plasma channel inside rails.

5.1.2 Motion of an arc plasma channel in modeling

The arc plasma channel sliding in rails is accelerated by Lorentz force of the rail gun. The circuit model for rail gun plasma reflects the acceleration due to $J \times B$ force related to the plasma mass and current. In general, the acceleration is proportional to the square of the discharge current. As shown in Figure 5.2, the simulation result of modeling is near to the experimental data. In addition, the discharge current is proportional to the magnitude of the initial charging voltage. Figure 5.3 shows the comparison of the plasma positions varying time evolution in experiment results and simulating results. The points of the experimental data present the results seen with the visual images via fast camera. Initial positions of actual plasma channel exist in locations ahead of the simulation results. It can be expected to reflect the gas injection velocity because the puffing gas is injected at the top of the rails. However, the ideal velocity of the modeling is faster than the experimental value through a slope of the graph. The difference of the velocity in rails seems to be caused by the drag force and frictional force on rails. Nevertheless, overall movement of the plasma channel is shown to be similar to the results of the simulation in the comparison.

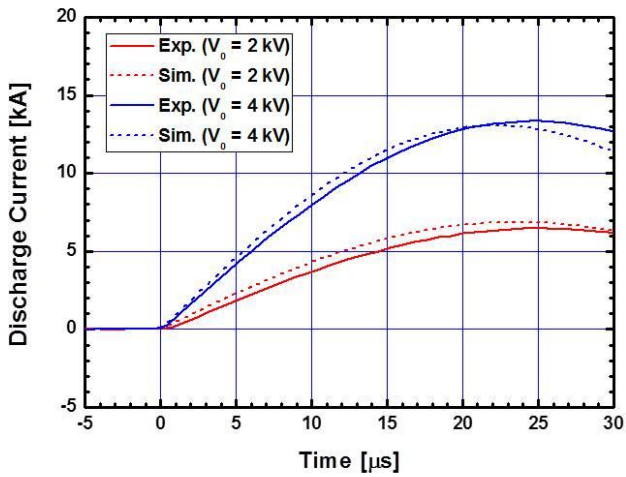

Figure 5.2 Comparison of the discharge currents in experiment results and simulating results.

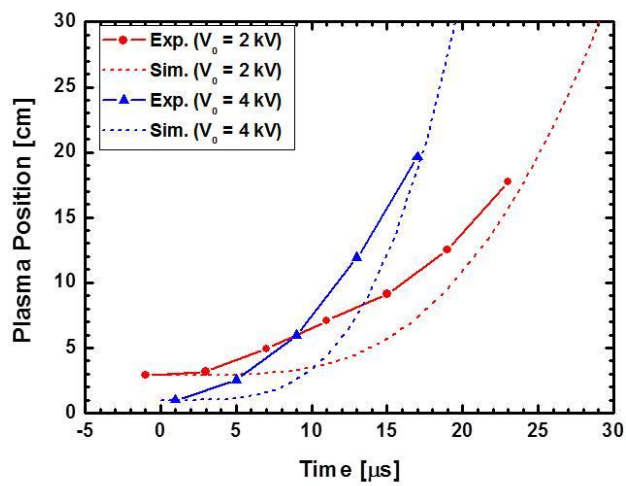

Figure 5.3 Comparison of the plasma positions varying time evolution in experiment results and simulating results.

5.2 Particle-In-Cell simulation of rail gun plasma jet

5.2.1 Simulation setup for PIC simulation

The modeling of plasma motion has much difficulty to many charged and neutral particles involved in behavior of the plasma. Furthermore, random collisions between them and external conditions cause many drawbacks. However, particle-in-cell (PIC) method [37] is introduced a very strong code in simulation of plasma in order to minimize complex problems. The code presents the motion of the particles in a cell divided by the grid. All the particles in the plasma are difficult and inefficient to simulate one by one computationally due to the high plasma density. For this reason, the super particle is used in the PIC simulation, because it represents as one particle of numerous particles.

OOPIC Pro is built on the XOOPIC physics kernel, an X11-based object oriented particle-in-cell code originally developed at the University of California at Berkeley [38]. It is a feature-rich 2D PIC simulator and designed to model plasmas, beams of charged particles, externally generated electric and magnetic fields, and low-to-moderate density neutral gases, using a wide variety of boundary conditions. It includes electrostatic and electromagnetic field solvers, as well as support for slab and cylindrical geometries. The OOPIC code is used to simulate the moving plasma jet ejected from the rail gun system in this research. Figure 5.4 presents boundary condition setup for PIC simulation. As for geometric setup, 2D simulation domain is selected in order to make up the motion of the plasma jet. The beam emitter and dielectric and conductor boundary, each of which has the same size as the experimental condition, are placed at the simulation domain.

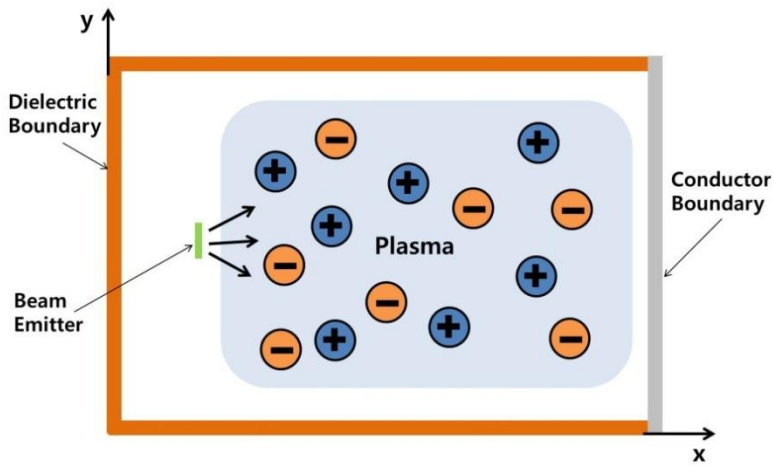

Figure 5.4 Schematic diagram of the 2D PIC simulation for rail gun plasma jet.

Table 5.1 shows the simulation conditions as for input parameters in the geometric setup. The input parameter, each of which has same values as the experimental conditions and results, are used in the simulation. Size of the simulation domain is 20 cm wide and 20 cm long. In this condition, 200 X 200 and $1x10^{-11}$ s are determined as the grid size and the time step, respectively. The grid size and time step should be well satisfied that the grid cell is smaller than the Debye length, and time step is less than reciprocal of the plasma frequency as shown in Eqs. (5.5) and (5.6).

$$\Delta x \le \lambda_D$$
$$\lambda_D = \sqrt{\frac{\varepsilon_0 k T_e}{n_e e^2}} \tag{5.5}$$

$$\Delta t \le \frac{1}{\omega_p}$$
$$\omega_p = \sqrt{\frac{e^2 n_0}{\varepsilon_0 m_e}} \tag{5.6}$$

where Δx is the spatial grid size, λ_D is the Debye length, Δt is the time difference, and ω_p is the plasma frequency. The super particle, number of physical particles to computer particles, is determined to represent $5x10^8$. The emitter length like distance between electrodes is 1 cm and the beam time emitting from it is $1x10^{-7}$ s. Also, the plasma temperature, density, and drift velocity for initial beam emission are like to the experimental results, respectively.

Table 5.1 Input parameters in OOPIC code.

Parameter	Input value
X-axis length [m]	0.2
Y-axis length [m]	0.2
Grid size	200x200
Emitter length [cm]	1
Beam emitting time [s]	$1x10^{-7}$
Time step [s]	$1x10^{-11}$
Super particles	$5x10^8$
Plasma Temperature [eV]	5
Plasma density [m-3]	$1x10^{19}$
Plasma velocity [km/s]	120

5.2.2 Results of the plasma jet motion using PIC simulation

Through the simulation conditions based on the experimental results, the PIC simulation is carried out. Each Figure 5.5 and 5.6 shows that the plasma jet is diffused in free space after emitting from the rail gun without magnetic field and with magnetic field, respectively. Without magnetic field, the plasma jet diffuses continuously in free space as shown in Figure 5.5. Eventually, the peak plasma density in the center of the plasma jet decreases gradually while the distribution is expanded. The simulation result is similar to the experimental result in case of hydrogen.

In order to troubleshoot for the plasma jet diffusion, it is used the magnetic field of 700 G in x-direction as shown in Figure 5.6. The most of the plasma jet particles are trapped in the magnetic field, and the particles move along the field. The narrowed density distribution relative to that of Figure 5.5 shows that the particles behave with collective motion. Through these simulation results, the experimental results can be validated, and the rail gun with the magnetic field like the simulation will be used to make the perfect shape of the plasma jet in future work.

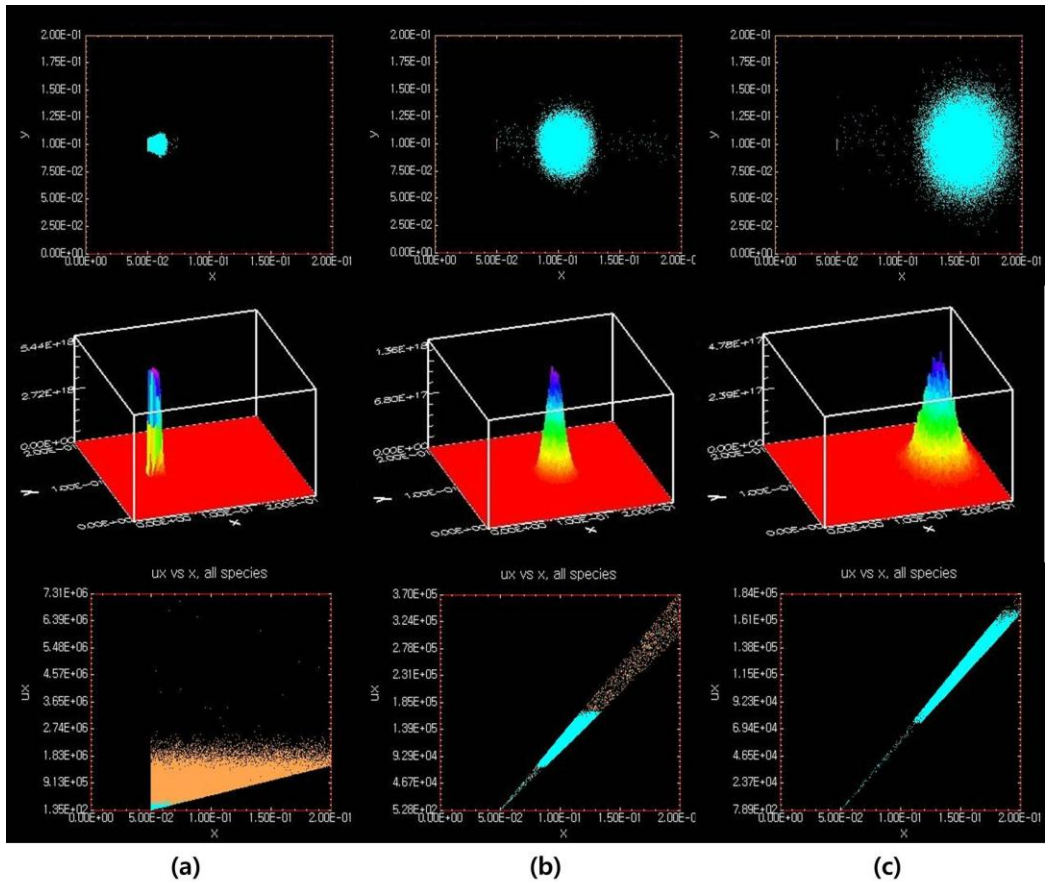

Figure 5.5 PIC simulation of a plasma jet diffused in free space after emitting from the rail gun without magnetic field. (top) Motion of the plasma jet, (middle) Plasma density distribution, and (bottom) Plasma velocity distribution at time of (a) 0.1 μs, (b) 0.5 μs, and (c) 0.9 μs from beam emission.

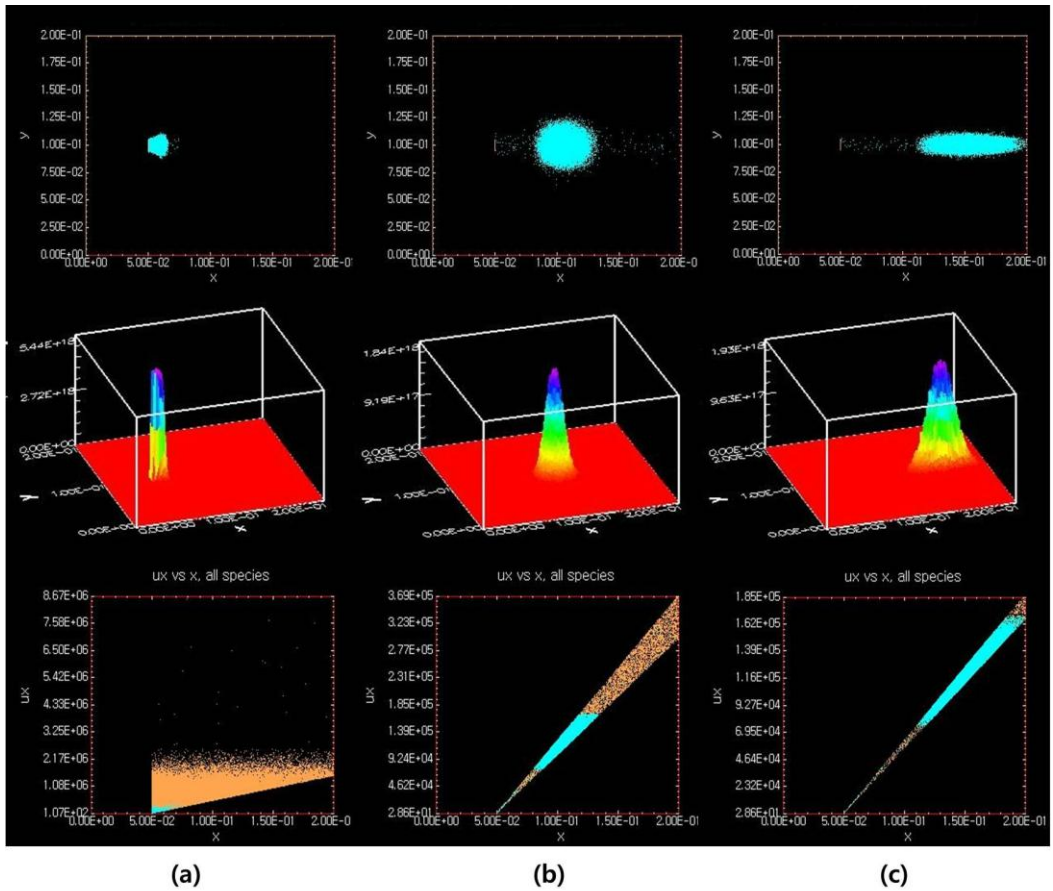

Figure 5.6 PIC simulation of a plasma jet diffused in free space after emitting from the rail gun with x-direction magnetic field of 700 G. (top) Motion of the plasma jet, (middle) Plasma density distribution, and (bottom) Plasma velocity distribution at time of (a) 0.1 μs, (b) 0.5 μs, and (c) 0.9 μs from beam emission.

Chapter 6 Conclusions and future work

In this thesis, characteristics of a rail gun plasma for simulating ELM-like plasma has been studied, with the design and fabrication of the rail gun and diagnostic systems and analysis of the experimental results. The rail gun plasma developed in the present work is characterized as the fast plasma jet with high density and ion velocity similar to ELM. In the case of argon, the peak density is measured to be approximately 3×10^{19} m^{-3} at a probe location of 112 mm apart from exit and each electron temperature and ion velocity is almost constant as around 3 eV and 11 km/s, respectively, at the time of peak density. The size of the jet in the flow direction is estimated as tens of centimeters from the time transient density profile. Similar results except for much higher ion velocity up to 100 km/s are obtained for hydrogen.

The jet parameters obtained by a lot of experiments are compared with the ELM parameters in ITER scale in terms of the electron density, ion velocity, and plasma size. The result shows that the plasma jet has the similar characteristics with real ELM plasma, and then it may be utilized as ELM-like plasma in simple laboratory environment. In addition, the outcome of H plasma jet parameters is available to use high heat flux test on the target, because the energy of the plasma jet can be made similar to impact energy of ELM plasma.

It is planned to improve the rail gun apparatus for generating more ELM-relevant plasma by changing rail electrodes to minimize impurities and installing the nozzle at the muzzle of the rail or the magnet arrays around the chamber to prevent the particle diffusion. Also, Additional diagnostics such as some more QLPs and photodiodes will be installed for the measurement of spatial shape of the plasma jet shape. In order to the control of the plasma jet, proper debunching simulation will be carried out for broadening plasma jet temporally or spatially via PIC code. Based on the simulation results, the

experimental control of the plasma jet using external electromagnetic fields is planning to be carried out in upcoming research.

Bibliography

[1] John Wesson, et al., *Tokamaks*, Clarendon Press-Oxford (2004).

[2] ITER Physics Basis, Nucl. Fusion 39 (1999).

[3] Loarte A, et al., *Power and particle control, Chapter 4*, Nucl. Fusion 47 (2005).

[4] A. Zhitlukhin, et al., *Effects of ELMs on ITER divertor armour materials*, Journal of Nuclear Materials 363-365 (2007).

[5] I. E. Garkusha, et al., Journal of Nuclear Materials 386-388 (2009).

[6] I. Sakuma, et al., IEEE/NPSS 24th Symposium on Fusion Engineering (2011).

[7] T. K. Gray, et al., ECA 29C. P-4.022 (2005).

[8] J. Rapp, et al., Fusion Engineering and Design 85 (2010).

[9] B. Pegourie, *Review: Pellet injection experiments and modeling*, Plasma Phys. Control. Fusion 49 (2007).

[10] R. A. Moyer, et al., *Edge localized mode control with an edge resonant magnetic perturbation*, Physics of Plasmas 12 (2005).

[11] Suttrop W., Plasma Phys. Control. Fusion 42 (2000).

[12] Loarte A., et al., Plasma Phys. Control. Fusion 45 (2003).

[13] K. Kamiya, et al., *Edge localized mode: recent experimental findings and related issures*, Plasma Phys. Control. Fusion 49 (2007).

[14] A. Kirk, et al., *Spatial and Temporal Structure of Edge-Localized Modes*, Physical Review Letters. Vol. 92, Num. 24 (2004).

[15] H. Zohm, *Edge localized modes (ELMs)*, Plasma Phys. Control. Fusion 38 (1996).

[16] S. Lisgo, et al., *Super-X advanced divertor design for MAST Upgrade*, 36th EPS Conference on Plasma Phys. Sofia. ECA Vol. 33E (2009).

[17] D. D. Ryutov, *Geometrical properties of a snowflake divertor*, Physics of Plasmas 14 (2007).

[18] C. F. Maggi, *Progress in understanding the physics of the H-mode pedestal and ELM dynamics*, Nucl. Fusion 50 (2010).

[19] C. S. Rashleighm, et al., *Electromagnetic Acceleration of Macroparticles to High Velocities*, Appl. Phys. 49(4) (1978).

[20] J. P. Barber, *The Acceleration of Macroparticles and a Hypervelocity Electromagnetic Accelerator*, Ph.D Thesis, The Australian National University (1972).

[21] J. Linke, et al., *High heat flux testing of plasma facing materials and components – Status and perspectives for ITER related activities*, Journal of Nuclear Materials 367-370 (2007).

[22] Masayoshi Nagata, et al., *Application of Magnetized Coaxial Plasma Guns for Simulation of Transient High Heat Loads on ITER Divertor*, IEEEJ Trans. 4 (2009).

[23] Sin-Li Chen, et al., *Instantaneous Direct-Display System of Plasma Parameters by Means of Triple Probe*, Journal of Applied Physics Vol. 36, No. 8 (1965).

[24] Adam K. Martin, et al., *A maximum-likelihood algorithm for reduction of Langmuir probe data*, Review of Scientific Instruments 78 (2007).

[25] Rodney L. Burton, et al., *Application of a Quadruple Probe Technique to MPD Thruster Plume Measurement*, Journal of Propulsion and Power Vol. 9, No. 5 (1993).

[26] Billy H. Johnson, et al., *Plasma Velocity Determination by Electrostatic Probes*, AIAA Journal Vol. 7, No. 10 (1969).

[27] A. Herrmann, et al., *The filamentary structure of ELMs in the scrape-off layer in ASDEX Upgrade*, Journal of Nuclear Materials 363-365 (2007).

[28] A. Kirk, et al., *Filament structure at the plasma edge on MAST*, Plasma Phys. Control. Fusion 48 (2006).

[29] N. Asakura, et al., *Parallel and radial transport of ELM plasma in the SOL and divertor of JT-60U*, Journal of Nuclear Materials 337-339 (2005).

[30] M. Kocan, et al., *First measurement of edge localized mode ion energies in the ASDEX Upgrade far scrape-off layer,* Plasma Phys. Control. Fusion 53 (2011).

[31] A. Kirk, et al., *Parameters determining the radial propagation of type-I edge localized modes (ELMs) in ASDEX Upgrade*, Plasma Phys. Control. Fusion 53 (2011).

[32] A. Kirk, et al., *Comparison of the spatial and temporal structure of type-I ELMs*, Journal of Physics: Conference Series 123 (2008).

[33] W. Fundamenski, et al., *ELM-wall interaction on JET and ITER*, Journal of Nuclear Materials 363-365 (2007).

[34] A. Kirk, et al., *Physics of ELM power fluxes to plasma facing components and implications for ITER*, Journal of Nuclear Materials 390-391 (2009).

[35] Victor Kowalenko, *A study of the equations of motion for a plasma-armature railgun*, Appl. Phys. 30 (1997).

[36] Zhi-Gang Shen, et al., *A study of a coaxial plasma gun*, Appl. Phys. 28 (1995).

[37] C. K. Birdsall, *Particle-In-Cell Charged-Particle Simulations, Plus Monte Carlo Collisions With Neutral Atoms, PIC-MCC*, IEEE Trans. Plasma Science. Vol. 19, No. 2 (1991).

[38] J. P. Verbonecoeur, et al., *An Object-Oriented Electromagnetic PIC Code*, Comput. Phys. Commun. 87 (1995).

Abstract in Korean

ELM 플라즈마 모사를 위한 레일건 플라즈마의 특성에 대한 연구

정경수

에너지시스템공학부

서울대학교 대학원

토카막에서는 H-mode 를 유지하면서 장시간 운전하는 것이 중요하지만, 일반적으로 고온 플라즈마 경계 면에서의 큰 압력 변화 때문에 불안정한 현상인 ELM (Edge Localized mode)이 발생하게 된다. 이렇게 불안정한 ELM 에 의한 다이버터 (Divertor)의 손상에 대한 연구는 핵융합로의 수명과 관련하여 해결해야 할 중요한 과제 중 하나이다. 기존의 ELM 모사 장치들은 대면 재료에 대해 큰 열 부하를 주어 그 변화를 관찰하고 재료를 선정하는 것을 목적으로 하였기 때문에 실제로 ELM 플라즈마의 특성을 잘 재현해내기보다는 고출력 에너지를 만드는 복잡한 형태의 빔 발생 장치이었다. 또한 이러한 모사 장치를 대면 재료 시험에만 제한적으로 사용하였다.

이에 본 논문에서는, ELM 과 유사한 플라즈마를 만들 수 있는 간단한 형태의 레일건 (rail gun)을 설계 및 제작하고, 실험과 전산모사를 통해 ITER 크기에서의 ELM 플라즈마의 밀도, 이온 유동 속도 측면에서 유사한 플라즈마 젯 (plasma jet)에 대한 연구를 수행하여 향후 다이버터에 ELM 플라즈마가 도달하기 전에 제어하는 연구에 기여하고자 하였다.

실험을 위해 일정한 방향으로 큰 로렌츠 힘을 발생시킬 수 있는 레일건 개념을 채택하였다. ELM 플라즈마의 특성을 바탕으로 전극 길이, 방전기체의 주입 시간, 충전 전압, 프로브 측정 위치와 같은 실험 조건들을 변화시키면서, ELM 과 유사한 특성을 지닌 플라즈마를 발생시킬 수 있는 조건들을 고려하여 ELM 모사에 적합한 레일건을 제작하였다. 진공 환경에서 각각의 아르곤과 수소 기체를 전극 사이의 공간에 주입하면서 높은 펄스 전압을 전극에 인가하여 레일 사이에서 방전을 일으켜 고속의 플라즈마 젯을 만들 수 있었다.

레일건에서 플라즈마 젯이 방출되기 전에 레일을 따라 이동하는 아크 플라즈마 채널에 대한 동적 특성을 확인하기 위하여 레일 전극 사이를 초고속 카메라로 진단하였다. 방전으로 발생한 플라즈마가 덩어리의 형태로 전극 사이를 가속하여 이동하는 것을 관찰할 수 있었고, 이것으로 대략적인 플라즈마 채널의 운동 속도를 추정할 수 있었다. 전류가 흐르는 레일과 전력 시스템을 하나의 간단한 회로 형태로 모델링하여 모사한 결과 플라즈마 채널의 이동 거리와 속도를 예측할 수 있었고, 이는 초고속 카메라의 진단 결과와 유의미한 수준으로 유사함을 검증할 수 있었다. 또한 전극 안 쪽 뿐만 아니라 전극에서 분출되는 순간의 플라즈마 젯의 형태를 초고속 카메라를 통해 확인할 수 있었다. 이것은 입자 거동을 전산 모사할 수 있는 OOPIC 을 통해 플라즈마 젯의 이동을 모사하여 비교하였다. 이러한 방식으로 플라즈마 젯의 형태와 초기 발생과정을 확인하였고, 레일건에서의 고속 플라즈마를

측정하기 적합한 4 중 랑뮤어 탐침을 제작하여 방전기체, 충전전압에 따라 플라즈마 젯을 거리별로 측정하였다. 각각의 탐침으로 수집되는 신호를 처리하기 위해 회로를 제작하여 탐침 간 전위차와 전류에 대한 데이터를 받았고, 데이터를 바탕으로 비선형 방정식을 풀어 플라즈마 젯의 전자 온도, 전자 밀도, 이온 속도를 계산하였다.

ELM 플라즈마의 입자를 제어하는 측면에서는 ELM 과 유사한 플라즈마 젯의 밀도, 속도, 크기가 중요한 요소이다. 진단된 아르곤 플라즈마 젯의 파라미터들은 실제 ELM 필라멘트 플라즈마 특성과 비교했을 때 온도를 제외하고는 큰 차이가 없었다. 특히 플라즈마 젯의 밀도와 드리프트 속도는 각각 $1\sim10\times10^{19}$ m^{-3} 와 10 km/s 이상 정도로 유사한 결과를 얻었고, 차후 플라즈마 입자를 전자기장으로 제어한다는 측면에서 봤을 때 실험실 환경에서 이 플라즈마 젯을 사용할 수 있을 것이다. 또한 진단된 수소 플라즈마 젯의 파라미터들 역시 실제 ELM 필라멘트의 플라즈마 특성과 비교했을 때 전자 밀도는 유사하지만 전자 온도가 상대적으로 매우 낮았다. 그러나 레일건의 로렌츠 힘을 이용하여 플라즈마 젯의 속도를 100 km/s 이상으로 만들어낼 수 있고, 충전 전압을 조절하여 원하는 속도로 올릴 수 있는 것이 가능함을 확인하였다. 실험에서의 플라즈마 속도에 대한 운동에너지로 실제 ELM 플라즈마의 대면 물질에 대한 충격 에너지와 유사하게 만드는 것이 가능할 것이다.

이와 같이 본 논문에서는 드리프트 속도와 에너지 측면에서 ELM 플라즈마에 근접한 특성을 지닌 플라즈마를 레일건을 이용하여 만들 수 있음을 확인할 수 있었다. 그러므로 향후 본 연구의 실험 환경에서 ELM 플라즈마와 유사한 특성을 가진 플라즈마 젯을 외부 전자기장을 이용하여

표적에 대한 부하를 감소시키는 연구를 진행하는데 기초가 될 것이고, 추가적으로 간단한 장치로 대면 재료 시험을 하는데도 활용될 수 있을 것이다.

주요어 : 레일건, ELM 플라즈마, 플라즈마 젯, 4 중 랑뮤어 탐침, 입자 전산모사, ELM 제어법

학번 : 2011-21107